. SCUOLA INTERNAZIONALE SUPERIORE DI STUDI AVANZATI

SISSA Digital Library

Cooling quasiparticles in A(3)C(60) fullerides by excitonic mid-infrared absorption

Original
Cooling quasiparticles in A(3)C(60) fullerides by excitonic mid-infrared absorption / Nava, A., Giannetti, C., Georges, A., Tosatti, E., Fabrizio, M.. - In: NATURE PHYSICS. - ISSN 1745-2473. - 14:2(2018), pp. 154-159. [10.1038/nphys4288]

Availability:
This version is available at: 20.500.11767/72025 since: 2018-04-05T09:42:37Z

Publisher:

Published
DOI:10.1038/nphys4288

Terms of use:

Testo definito dall'ateneo relativo alle clausole di concessione d'uso

Publisher copyright

note finali coverpage

(Article begins on next page)

11 September 2026

arXiv:1704.05613v1 [cond-mat.str-el] 19 Apr 2017

Cooling quasiparticles in A_3C_{60} fullerides by excitonic mid-infrared absorption

Andrea Nava,[1] Claudio Giannetti,[2] Antoine Georges,[3,4,5] Erio Tosatti,[1,6,7] and Michele Fabrizio[1]

[1] *International School for Advanced Studies (SISSA), Via Bonomea 265, I-34136 Trieste, Italy*

[2] *Interdisciplinary Laboratories for Advanced Materials Physics (ILAMP), Università Cattolica del Sacro Cuore, Brescia I-25121, Italy*

[3] *Centre de Physique Théorique, Ecóle Polytechnique, CNRS, Université Paris-Saclay, 91128 Palaiseau, France*

[4] *Collége de France, 11 place Marcelin Berthelot, 75005 Paris, France*

[5] *Department of Quantum Matter Physics, University of Geneva, 24 Quai Ernest-Ansermet, 1211 Geneva 4, Switzerland*

[6] *CNR-IOM Democritos, Via Bonomea 265, I-34136 Trieste, Italy*

[7] *International Centre for Theoretical Physics (ICTP), Strada Costiera 11, I-34151 Trieste, Italy*

Long after its discovery superconductivity in alkali fullerides A_3C_{60} still challenges conventional wisdom. The freshest inroad in such ever-surprising physics is the behaviour under intense infrared (IR) excitation. Signatures attributable to a transient superconducting state extending up to temperatures ten times higher than the equilibrium $T_c \sim 20$ K have been discovered in K_3C_{60} after ultra-short pulsed IR irradiation – an effect which still appears as remarkable as mysterious. Motivated by the observation that the phenomenon is observed in a broad pumping frequency range that coincides with the mid-infrared electronic absorption peak still of unclear origin, rather than to TO phonons as has been proposed, we advance here a radically new mechanism. First, we argue that this broad absorption peak represents a "super-exciton" involving the promotion of one electron from the t_{1u} half-filled state to a higher-energy empty t_{1g} state, dramatically lowered in energy by the large dipole-dipole interaction acting in conjunction with Jahn Teller effect within the enormously degenerate manifold of $(t_{1u})^2(t_{1g})^1$ states. Both long-lived and entropy-rich because they are triplets, the IR-induced excitons act as a sort of cooling mechanism that permits transient superconductive signals to persist up to much larger temperatures.

Superconducting alkali doped fullerenes A_3C_{60} are molecular compounds where several actors play together to determine an intriguing physical behaviour. The high icosahedral symmetry of C_{60}

implies, prior to intermolecular hybridisation, a large degeneracy of the molecular orbitals, thus a strong electronic response to JT molecular distortions lowering that symmetry. In particular, the t_{1u} LUMO, which accommodates the three electrons donated by the alkali metals, is threefold degenerate and JT coupled to eight fivefold-degenerate molecular vibrations of H_g symmetry, which mediate the pairing[1]. The JT effect, favouring low spin, is partly hindered by (Coulomb) Hund's rule exchange, which favours high spin. Therefore the overall singlet pairing strength g, though still sizeable, is way too small compared to the charging energy of each C_{60}^{3-} to justify by simple arguments why A_3C_{60} are s-wave superconductors. The explanation of this puzzle proposed in [2, 3] and vindicated by recent experiments emphasises the crucial role of a parent Mott insulating state where the JT coupling effectively inverts Hund's rules, the molecular ground state therefore turning to spin $S = 1/2$ rather than $S = 3/2$ [4]. A $S = 1/2$ antiferromagnetic insulating phase is indeed the ground state in over-expanded $NH_3K_3C_{60}$[5, 6] and in Cs_3C_{60}[7] at ambient pressure. In the metallic state, attained under pressure in Cs_3C_{60} and at ambient pressure in K_3C_{60} and Rb_3C_{60}, the incipient Mott localisation slows down the coherent motion of quasiparticles while undressing them from charge correlations. As a result, the singlet pairing strength g eventually overwhelms the quasiparticle Coulomb pseudopotential and, on approaching the Mott transition, the system is effectively driven towards the top of the universal T_c *vs.* g curve [8], where the critical temperature reaches the maximum possible value at a given non-retarded attraction $T_c^{\mathrm{MAX}} \sim 0.055\, g$. Thus, according to the theory of Ref. [3], the peak $T_c \sim 38$ K reached by Cs_3C_{60} at ~ 7 kbar [9, 10] is actually the highest attainable at equilibrium in fullerides.

This equilibrium upper limit has been far surpassed in out-of-equilibrium conditions in a recent remarkable pump-probe experiment on K_3C_{60}[11]. After irradiation by an intense femtosecond infrared pulse between 80 and 200 meV, K_3C_{60} showed a transient regime of some picoseconds where the optical properties looked like those of a superconductor, alas up to a temperature $T \gtrsim 200$ K, ten times higher than the equilibrium $T_c \sim 20$ K, see Fig. 1(b). This tantalising observation has already elicited various theoretical efforts [12–16], where it was mainly assumed, as in the original work [11], that TO phonon IR absorption acts as the crucial ingredient increasing the pairing efficiency. Here we follow another route directly inspired by experimental features, which leads to a totally different perspective.

First of all, the transient "superconducting" gap does increase [11], yet not as much as the transient T_c, see Fig. 1(b). More importantly, we note in Ref. [11] that the transient reduction of optical conductivity (suggestive of a transiently enhanced superconducting state) is broadly

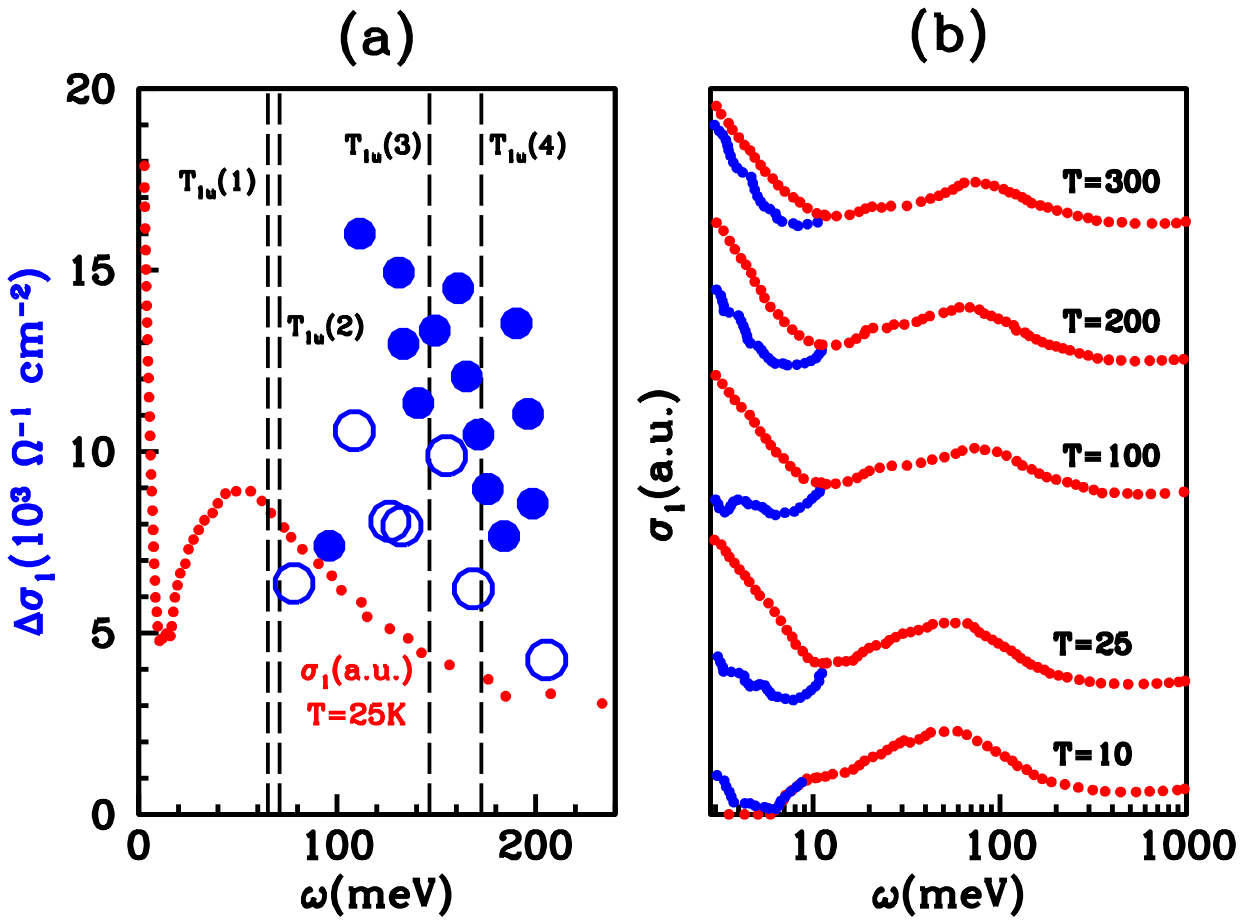

FIG. 1: **Experimental data from Ref. [11]. (a) Blue circles: spectral-weight reduction, $\Delta\sigma_1(\omega)$, in the optical conductivity as a function of the laser frequency ω from different measurements (data from Fig. 4d of Ref. [11]). Red dots: equilibrium optical conductivity at $T = 25$ K with the broad IR peak which we interpret as involving a $(t_{1u})^3 \cup (t_{1u})^2(t_{1g})^1$ exciton. Dashed vertical lines: frequencies of the T_{1u} TO phonon modes. Note that, except at two lowest frequency points, $\Delta\sigma_1(\omega)$ follows closely the shape of the mid IR absorption peak, rather than peaking at the T_{1u} frequencies. (b) Optical conductivities at equilibrium, red dots, and 1 ps after the photoexcitation, blue dots, for different temperatures, below, $T = 10$ K, and above, $T = 25, 100, 200, 300$ K the equilibrium T_c (data from Figs. 2b, 2e, 3b, 3e and from Extended data figure 9e of Ref. [11])**

distributed over the IR pumping frequency range from 80 to 200 meV, see Fig. 1(a). Although that includes the two highest T_{1u} IR-active modes near 150 and 170 meV[17], the enhancement does not especially peak there, extending instead to lower frequencies, see Fig. 1(a). There is instead an intriguing similarity between a long known [18, 19] broad absorption peak that characterises the equilibrium IR response of K_3C_{60} and Rb_3C_{60}. This peak is present and strong in the equilibrium optical data of Ref. [11], centred around ~ 50 meV and ~ 100 meV broad, see Fig. 1(b). Given these characteristics, the underlying excitation is not a phonon, and can only be electronic; yet,

nobody seems to know exactly what it is [20–23].

Intriguingly, it now appears that the superconducting enhancement follows rather closely the shape of this IR absorption feature. Our first task is therefore to understand this excitation which might provide a precious clue to superconductivity enhancement in alternative to the resonance with infrared-active TO modes.

In A_3C_{60} the conduction electrons occupy the narrow band originated by the threefold degenerate t_{1u} LUMO of C_{60}. The Coulomb interaction projected onto the t_{1u} manifold includes a charge repulsion, the Hubbard $U \sim 1$ eV, plus a quadrupole-quadrupole electronic interaction providing an intra-molecular Hund's rule exchange $J_{\rm H} > 0$. The latter splits the twenty possible $(t_{1u})^3$ configurations of C_{60}^{3-}, assumed at first with nuclei rigidly frozen in their ideal icosahedral positions, as

$$\begin{aligned} E\left({}^2T_{1u}\right) - E\left({}^4A_u\right) &= 10\, J_{\rm H}\,, \\ E\left({}^2H_u\right) - E\left({}^4A_u\right) &= 6\, J_{\rm H}\,. \end{aligned} \tag{1}$$

The highest-spin state, ${}^4A_u$, has therefore the lowest energy, see Table I. Once the nuclei defreeze, and the molecular ion can distort, the resulting JT energy E_{JT} strongly competes against exchange $J_{\rm H}$, since now the quadrupole operators of the t_{1u} electrons couple with the quadrupole of the H_g vibrational modes, but with opposite sign. [3] In C_{60}^{3-}, the JT effect actually prevails over Coulomb exchange, effectively inverting Hund's rules. The real ground state thus becomes the low-spin ${}^2T_{1u}$ multiplet[24–29].

Next, what about the $(t_{1u})^2(t_{1g})^1$ configuration? Within each C_{60}^{3-} molecule, the lowest dipole-allowed excitation corresponds to transferring one electron from the t_{1u} LUMO to the t_{1g} LUMO+1, which is also threefold degenerate and whose single-particle energy level lies $\Delta\epsilon \sim 1.2$ eV above. High as this energy is, the $(t_{1u})^2\,(t_{1g})^1$ subspace comprises as many as 90 states, hence many times more susceptible to exchange splitting and JT effects than the lowest energy $(t_{1u})^3$ subspace. In addition, the Coulomb interaction projected onto the enlarged t_{1u}–t_{1g} manifold also includes a dipole-dipole interaction, which is stronger than the quadrupole-quadrupole. Through a fully quantitative multipole expansion of the Coulomb interaction, Nikolaev and Michel found (omitting JT couplings)[30] that the split $(t_{1u})^2\,(t_{1g})^1$ subspace spans a gigantic 2 eV range, four times wider than the splitting $10J_{\rm H} \simeq 476$ meV of the $(t_{1u})^3$, see Table I. The two lowest $(t_{1u})^2\,(t_{1g})^1$ states with symmetry ${}^4H_g$ and ${}^2T_{1g}$ lie at only 494 meV and 525 meV, respectively, above the ${}^4A_u$ ground state [31], and that is before JT coupling. After allowing for JT, there is a further lowering, and the situation becomes richer [32, 33]. The quadrupole moment of the t_{1g} LUMO+1 has opposite

E(meV)	$(t_{1u})^3$	$(t_{1u})^2(t_{1g})^1$
0	${}^4A_u$	
285	${}^2H_u$	
476	${}^2T_{1u}$	
494		${}^4H_g$
525		${}^2T_{1g}$
618		${}^4A_g$
1109		${}^2G_g + {}^2T_{2g}$
1143		${}^4T_{1g}$
1280		${}^2H_g$
1496		${}^2T_{1g}$
1947		${}^2H_g$
2218		${}^2A_g$
2549		${}^2T_{1g}$

TABLE I: **Molecular terms of** *undistorted* $\mathbf{C_{60}^{3-}}$ **calculated in the absence of Jahn Teller coupling within the** $(t_{1u})^3 \cup (t_{1u})^2(t_{1g})^1$ **manifold according to the interaction model III of Ref. [30]. The zero of energy is set at the lowest** ${}^4A_u$ **state and the single-particle energy difference between** t_{1g} **and** t_{1u}**,** $\Delta\epsilon = 1153\,$**meV, is the same as in [30]. The electronic configurations are labeled according to the irreducible representations of the icosahedral group** I_h**. Since the** t_{1u} **and** t_{1g} **orbitals transform as atomic** p **orbitals, they are in one to one correspondence with angular momentum states in** $O(3)$ **symmetry:** $A \to S$**,** $T \to P$**,** $H \to D$ **and** $G + T \to F$**. Note the exceptionally wide spread of terms in the** $(t_{1u})^2(t_{1g})^1$ **configuration.**

sign to the t_{1u} LUMO, and its absolute value is 2.6 times larger, which makes JT couplings much more effective. In particular, and unlike the $(t_{1u})^3$ manifold, the JT effect in $(t_{1u})^2\,(t_{1g})^1$ is stronger in the high-spin $S = 3/2$ subspace than in low-spin $S = 1/2$. The reason is that in the $S = 3/2$ subspace the H_g vibrations couple together the lowest energy ${}^4H_g$ with the ${}^4A_g$ term, which is a mere 124 meV above, see Table I. In the $S = 1/2$ subspace, by contrast, the lowest energy ${}^2T_{1g}$ is only coupled to states higher than 600 meV above, which reduces the effect.

We further note that the new $t \otimes H$ $(t_{1u})^2\,(t_{1g})^1$ JT problem within configurations ${}^4H_g$ and ${}^4A_g$ is equivalent to that of C_{60}^{2-} in the $S = 0$ subspace of the $(t_{1u})^2$ manifold, which involves the configurations ${}^1H_g$ and ${}^1A_g$ and where the JT energy gain is known to be maximum [24–26, 28]. On the other hand, the Coulomb exchange splitting $E({}^4A_g) - E({}^4H_g) = 124\,$meV of $(t_{1u})^2\,(t_{1g})^1$ $S = 3/2$ subspace is smaller than $E({}^1A_g) - E({}^1H_g) = 6J_{\rm H} = 286\,$meV of the $S = 0$ $(t_{1u})^2$ case, implying a larger JT energy gain.

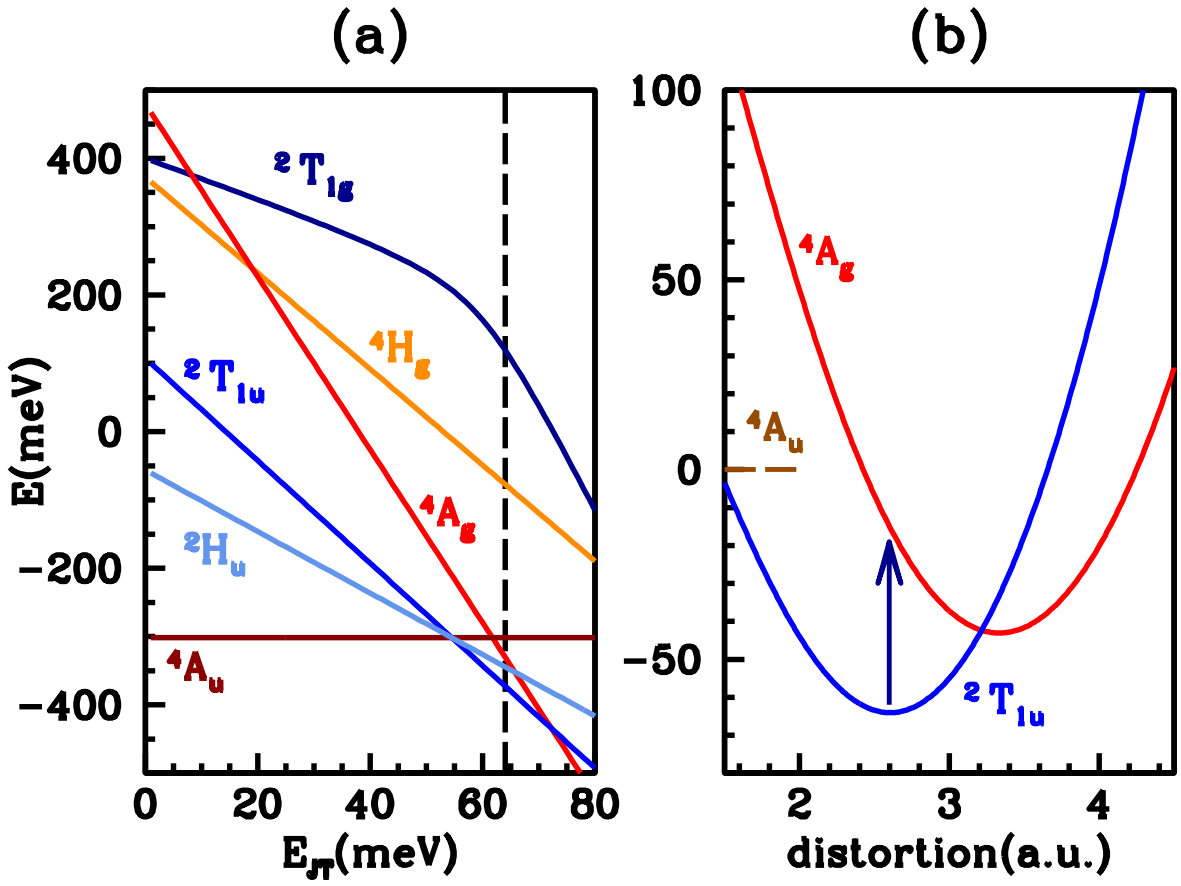

FIG. 2: **Molecular terms in the presence of Jahn-Teller. Panel (a): Low-lying C_{60}^{3-} molecular terms as function of the t_{1u} JT energy $E_{\rm JT}$ in the antiadiabatic approximation. Ungerade (u) and gerade (g) terms derive from $(t_{1u})^3$ and from $(t_{1u})^2(t_{1g})^1$ configurations, respectively. Terms are calculated as in Table I, now with effective exchange parameters including JT contributions evaluated in the anti-adiabatic approximation (see Supplementary Notes). The Coulomb exchange parameters such as $J_{\rm H}$ are the same as in Table I with a 14% reduction to mimic screening effects. The t_{1g} JT energy is taken as $1.25^2\,E_{\rm JT}$ and $\Delta\epsilon = 1240\,$meV to account for the overestimate of the t_{1g} downward single-particle energy-shift within the antiadiabatic approximation. The vertical dashed line indicates the suggested appropriate parameter for K_3C_{60}. Panel (b): Energy as a function of the modulus of the JT distortion of the $^2T_{1u}$ and ^4A_g configurations. The zero of energy is set at the ^4A_u level and we take $\Delta\epsilon = 1080\,$meV and an interaction screening reduction of 22%. The calculation is performed within the single mode approximation by the variational approach of Ref. [28] using a mode frequency $\omega = 100\,$meV, vibrational coupling $g = 1.32$ for t_{1u}, which corresponds to $E_{\rm JT} = 87\,$meV, and $1.25\,g$ for t_{1g}. The differences in screening reduction and $\Delta\epsilon$ with respect to the left panel take into account the overestimated JT effect within the antiadiabatic approximation. The arrow shows the vertical Franck-Condon exciton transition.**

Accurate estimates of the molecular terms within the enlarged $(t_{1u})^3 \cup (t_{1u})^2(t_{1g})^1$ manifold and in

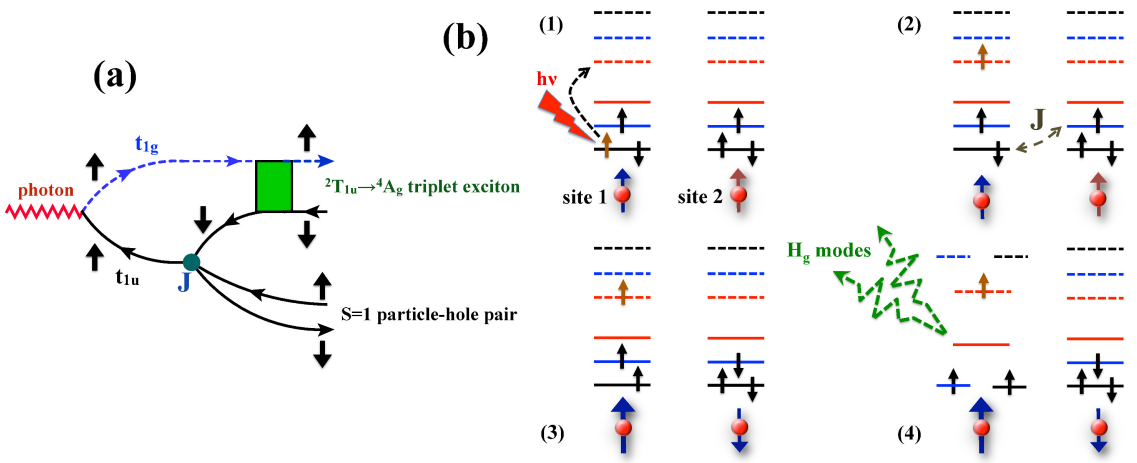

FIG. 3: **The absorption process. Panel (a): diagrammatic representation of the absorption. The photon induces a virtual dipolar transition $t_{1u} \to t_{1g}$. This intermediate state spawns a triplet super-exciton and a spin-triplet particle-hole pair. The high density of the latter near a Mott transition boosts the strength of this process. The circular vertex J is the *intermolecular* four-leg vertex exchange, the square electron-hole interaction comprises intramolecular exchange, JT and Franck-Condon effects, and all t_{1u} (solid black lines) and t_{1g} (dashed blue ones) Green's functions include self-energy corrections. Panel (b): pictorial representation of the same process with the absorption of a paramagnon. In the initial state (1) two sites are both in the $^2T_{1u}$ configuration, here drawn in the static JT limit. Note that site 2 is in a spin-state disfavoured by the inter-site antiferromagnetic exchange, i.e. a paramagnon excitation is assumed to be present. The photon with energy $h\nu$ transfers a t_{1u} electron (solid levels) into the t_{1g} orbitals (dotted levels). Note that the JT distortion of the t_{1u} orbitals is opposite to that of t_{1g}, as highlighted by the colours of the orbitals. In (2) $\to$ (3) the antiferromagnetic exchange J flips the spins of the two sites, 1 and 2, so that site 2 has now the right antiferromagnetic spin direction: the paramagnon has been absorbed. Through the emission of H_g vibrations, site 1 relaxes to the optimal JT distortion corresponding to the state ^4A_g.**

presence of JT coupling to the H_g vibrations would require a precise knowledge of all Hamiltonian parameters that are involved. That's a tall order, because, while the frequencies of the H_g modes are known from experiments, and different calculations of JT energy E_{JT} more or less agree, the individual values of the coupling constants with the t_{1u} electrons are hard to establish [34] without resorting to photoemission experiment [35]. Also questionable is whether the simple linear coupling to vibrations, as usually assumed, is sufficient, as has been pointed out [36, 37]. Besides that, there are so far no direct estimate of the H_g vibration coupling constants with the t_{1g} electrons, obviously not extractable from photoemission. We mentioned that the t_{1g} quadrupole moment is larger in absolute value than the t_{1u} one, which would suggest stronger vibration coupling constants, as

indeed observed in electronic structure calculations of isolated molecular anions [38]. Moreover, t_{1g} electrons couple preferentially to higher frequency H_g vibrations with tangential character, while t_{1u} electrons to lower frequency radial vibrations, which might also imply a larger t_{1g} JT energy [36]. One should finally note that, given the large size of the $(t_{1u})^2(t_{1g})^1$ subspace, even small variations of the many Coulomb exchange parameters[30] and vibrational coupling constants may lead to appreciably different results.

For these reasons we opt for a less ambitious approach and, following Ref. [3], we treat the JT problem within the anti-adiabatic approximation, were all effects depend only on the value of the total JT energy gain $E_{\rm JT}$, whose value for t_{1u} electrons is far less uncertain than the value of each vibrational coupling constant [34], see the Supplementary Notes for details. We use the model III interaction parameters of Nikolaev and Michel[30], with a 14% reduction to account for screening effects of nearby molecules[39], and we further assume, in accordance with the density functional results of [38], that the t_{1g} LUMO+1 JT energy is 1.25^2 larger than the t_{1u} LUMO one. In the left panel of Fig. 2 we show the low lying molecular terms as function of $E_{\rm JT}$ [34].

We can now consider the full multiplet spectrum for a realistic estimate of $E_{\rm JT} = 50 - 70\,{\rm meV}$ [34]. The ${}^2T_{1u}$ ground state and the lowest ${}^2H_u$ excitation, whose role was recently discussed [29], both belong to the $(t_{1u})^3$ manifold. The very next state however is the ${}^4A_g$ term, of $(t_{1u})^2\,(t_{1g})^1$ origin, dramatically pushed down close to the ground state by JT and dipole-dipole interaction, despite the 1 eV energy of the t_{1g} LUMO+1. We also performed a different calculation, treating the JT coupling within the single mode approximation [40] and using a variational approach [28] that consists of a statically distorted wavefunction projected onto a state with well defined icosahedral symmetry (details are in the Supplementary Notes). In the right panel of Fig. 2 we show the energies thus obtained of the ${}^2T_{1u}$ and ${}^4A_g$ states as function of the distortion vector norm. As anticipated, the ${}^4A_g$ energy minimum is reached for a larger distortion than that of ${}^2T_{1u}$, which entails substantial Franck-Condon effects - further strengthened by the shape difference, bimodal for ${}^2T_{1u}$ [24, 25] and unimodal for ${}^4A_g$.

We propose that the IR peak observed in A_3C_{60} corresponds precisely to the low lying ${}^4A_g$ state, the ${}^2T_{1u} \rightarrow {}^4A_g$ transition essentially turning into a genuine triplet exciton in the bulk material. The parity allowed but spin forbidden optical creation of this exciton can actually acquire oscillator strength and appear in the IR optical spectrum of a narrow-band nearly (antiferro)magnetic metal, through the simultaneous absorption/emission of a low energy spin-triplet particle-hole excitation, that is a paramagnon. For that it is important to recall that A_3C_{60} are indeed narrow quasiparticle-band metals, close to a transition into an antiferromagnetic Mott insulator state, so much so

that the transition is realised when *the cation A* merely changes from Rb to Cs. The absorption process is schematically shown in Fig. 3. The photon induces a virtual spin-conserving transition $t_{1u} \rightarrow t_{1g}$. This intermediate state then transforms into the triplet exciton by absorbing/emitting a paramagnon via intermolecular exchange. One should note that this absorption mechanism is of the very same nature to that introduced by Rice and Choi [41], which is necessary to explain why uncharged T_{1u} vibrations acquire oscillator strength and thus are observed in optics. The contribution of the ${}^2T_{1u} \rightarrow ({}^4A_g \pm \text{paramagnon})$ peak to the optical conductivity reads

$$\delta\sigma_1(\omega) \propto \int_0 d\epsilon\, \mathcal{A}_{\text{exc}}(\epsilon) \Big[\theta(\epsilon-\omega)\, b(\epsilon-\omega)\, \chi"(\epsilon-\omega) + \theta(\omega-\epsilon) \Big(1 + b(\omega-\epsilon)\Big) \chi"(\omega-\epsilon) - b(\epsilon+\omega)\, \chi"(\epsilon+\omega) \Big], \tag{2}$$

where $\mathcal{A}_{\text{exc}}(\epsilon)$ is the exciton absorption spectrum, $b(\epsilon)$ the Bose distribution function, and $\chi"(\epsilon)$ the imaginary part of the dynamical local spin susceptibility. Equation (2) suggests that the large width of the absorption peak, which experimentally corresponds to a timescale of about 7 fs, is the result of a convolution between the paramagnon bandwidth and a Franck-Condon broadening, rather than a radiative lifetime of the exciton. In fact, the expectedly strong Franck-Condon effect must cause a large broadening in $\mathcal{A}_{\text{exc}}(\epsilon)$ corresponding to the non-radiative relaxation of the triplet exciton to a dark state whose lifetime might be much longer, possibly picoseconds or more, before eventual (phosphorescent) recombination. In agreement with this exciton-paramagnon interpretation, the IR absorption peak grows in importance and intensity from K_3C_{60} to Rb_3C_{60}[18], the latter closer to Mott insulation (realised in Cs_3C_{60}), thus with stronger and narrower paramagnons.

The next and central question in the present context is if and why this exciton peak should actually play a role in the apparent enhancement of T_c found by Ref. [11] where IR-pumping is roughly in the same frequency range. We start by noting that the experimental transient superconducting-like absorption spectra suggest, see Fig. 1(b), that the IR pump can act to sweep away the thermally excited quasiparticle states that, at equilibrium, are responsible for the gap filling-up and closing with the transition to the normal state. Things superficially seem as if the pump effectively cooled down quasiparticles. Following this hypothesis, we can qualitatively describe how the quasiparticle distribution should evolve first during the IR laser pulse, about 300 fs long. Within that short time lapse, the system is effectively isolated from the environment, with which it was in thermal equilibrium before the IR shot. The IR pulse supplies the initial normal metal with energy, which is sunk in the exciton-paramagnon excitation as well as by the vibrations that are emitted dur-

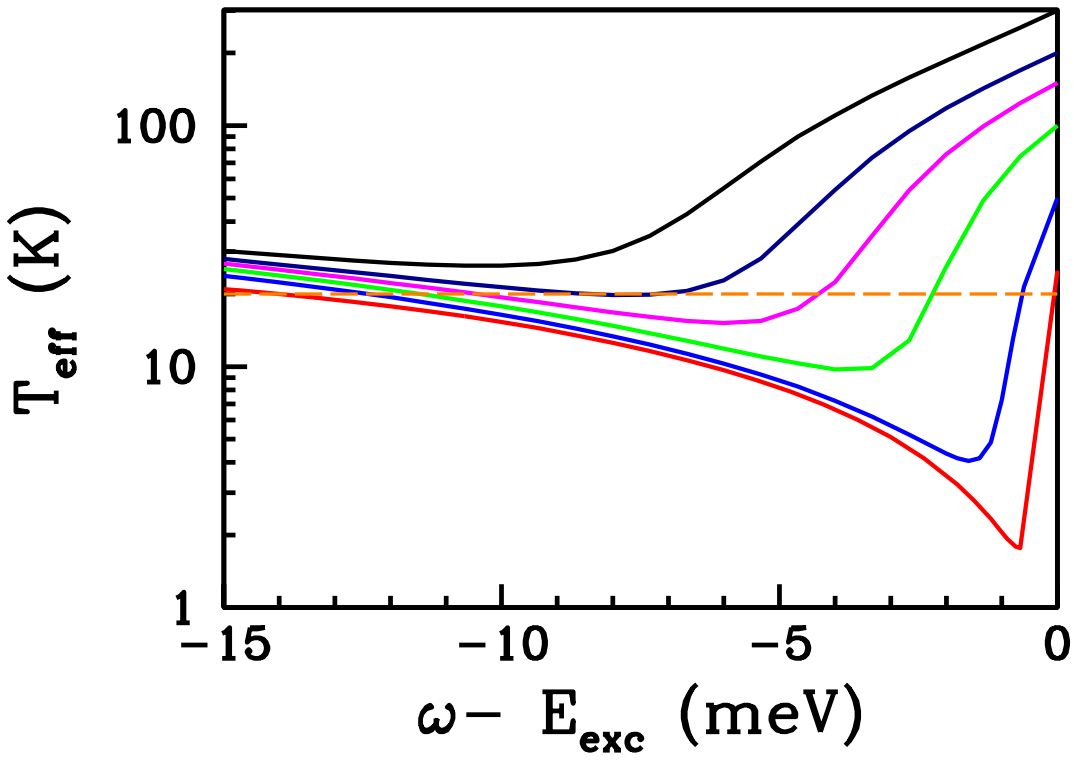

FIG. 4: **Effective temperature $T_{\rm eff}$ after the laser pulse calculated as explained in the main body of the text, for initial values $T = 300, 200, 150, 100, 50, 25$ K, from the top curve (black) to the bottom one (red), as function of $\omega - E_{\rm exc}$, where ω is the light frequency, with an assumed quasiparticle bandwidth of 100 meV and a sharp exciton line. The coefficient that multiplies the process in Fig. 3 is fixed to reproduce in linear response the excitonic peak value of the optical conductivity at equilibrium. The horizontal line at 20 K is the value of the equilibrium T_c**

ing the molecular relaxation after the vertical Franck-Condon transition. If we assume that the quasiparticle collision rate is high enough, as expected by the poor Fermi-liquid character above T_c [3], then the quasiparticle subsystem will exit the laser shot time in an effective microcanonical ensemble identified by an energy $\mathcal{E}$ and quasiparticle number $\mathcal{N}$. At a later time the quasiparticles will eventually come to equilibrium with the excitons, the lattice and the molecular vibrations (the decay times of the eight H_g modes into t_{1u} particle-hole excitations range between 0.03 and 4 ps). Yet, in the long transient before that happens, we can legitimately define an entropy $\mathcal{S}(\mathcal{E},\mathcal{N})$ of the quasiparticle liquid and its effective temperature $T_{\rm eff}^{-1} = \partial\mathcal{S}/\partial\mathcal{E}$. Moreover, if the quasiparticle collision integral is strong enough to establish local equilibrium during the whole pulse duration,

we are additionally allowed to define an entropy $S\big(\mathcal{E}(t),\mathcal{N}(t)\big)$ that depends on the quasiparticle energy, $\mathcal{E}(t)$, and number, $\mathcal{N}(t)$, at time t after the pulse front arrives. The absorption process of Fig. 3 implies that the creation rate of excitons is

$$\dot{N}_{\rm exc}(t) = \int d\epsilon\, \mathcal{A}_{\rm exc}(\epsilon)\, \dot{n}_{\rm exc}(\epsilon,t)\,, \tag{3}$$

where $\dot{n}_{\rm exc}(\epsilon,t)$ is equal to the term in square brackets of Eq. (2) multiplied by a parameter that we fit from equilibrium optical data (see Supplementary Notes), with the Bose distribution function and magnetic susceptibility corresponding to the instantaneous local equilibrium conditions. Since at $\omega \leq E_{\rm exc}$, for each extra exciton a quasiparticle is annihilated then $\dot{N}_{\rm exc}(t) = -\dot{\mathcal{N}}(t)$. Moreover energy conservation implies that

$$\dot{\mathcal{E}}(t) = \int d\epsilon\, \big(\omega-\epsilon\big)\, \mathcal{A}_{\rm exc}(\epsilon)\, \dot{n}_{\rm exc}(\epsilon,t) = \big(\omega - E_{\rm exc}\big)\, \dot{N}_{\rm exc}(t)\,, \tag{4}$$

where ω is the laser frequency and the last equivalence holds if $\mathcal{A}_{\rm exc}(\epsilon) \sim \delta(\epsilon - E_{\rm exc})$, which we shall assume hereafter for simplicity. Because of our assumption of local equilibrium, it follows that the quasiparticle entropy satisfies

$$T(t)\,\dot{\mathcal{S}}(t) = \dot{\mathcal{E}}(t) - \mu(t)\,\dot{\mathcal{N}}(t) = \int d\epsilon\, \big(\omega-\epsilon+\mu(t)\big)\, \mathcal{A}_{\rm exc}(\epsilon)\, \dot{n}_{\rm exc}(\epsilon,t) = \Big(\omega - E_{\rm exc} + \mu(t)\Big)\, \dot{N}_{\rm exc}(t)\,, \tag{5}$$

where $T(t)$ and $\mu(t) = -T(t)^{-1}\big(\partial\mathcal{S}/\partial\mathcal{N}\big)_{\mathcal{E}}$ are, respectively, the instantaneous temperature and chemical potential. The entropy is expected to be maximum when the number of t_{1u} quasiparticles is equal to its initial value of three per molecule, so that $\mu(t) < 0$ for any $\mathcal{N}(t) < \mathcal{N}(0)$. Through Eq. (5) we thus reach the conclusion that the quasiparticle entropy can indeed decrease, and so the effective temperature, especially for frequencies $\omega \leq E_{\rm exc}$ when exciton creation requires absorption of thermal quasiparticle-quasihole triplet pairs. To simplify the calculation of $T_{\rm eff} = T(t \simeq 300$ fs) at the end of the laser pulse, besides assuming $\mathcal{A}_{\rm exc}(\epsilon) \sim \delta(\epsilon - E_{\rm exc})$, we also neglect the contribution from the change in quasiparticle density, i.e. we take $\mu(t) = 0$ in (5), which implies that the entropy may decrease only below resonance. Furthermore we assume for $\chi''(\epsilon)$ the expression of non-interacting quasiparticles at half-filling and temperature $T(t)$ with a reduced bandwidth of 100 meV, and model the evolution of their distribution function by a Boltzmann type of equation (see Supplementary Notes). In Fig.4 we show $T_{\rm eff}$ thus obtained for equilibrium sample temperatures $T = 25, 50, 100, 150, 200, 300$ K. The result of this modelling, crude but we believe inevitable, is that the effective temperature $T_{\rm eff}$ can indeed be substantially lower than the equilibrium value – thermal triplet quasiparticle-quasihole pairs being absorbed so that IR pumping can reach the exciton energy.

Conclusions – The apparently tenfold critical temperature enhancement discovered by IR pumping in K_3C_{60} [11] is explained by a novel mechanism. First, noting that the effect broadly overlaps in frequency with the unexplained equilibrium mid-infrared absorption peak observed in all A_3C_{60} fullerides, that peak is argued, on the basis of single-molecule calculations, to correspond to the creation of a triplet exciton, Frank-Condon broadened and downshifted from its high LUMO–LUMO+1 energy by large intra-molecular interactions. Spin conservation requires this process to be accompanied by absorption/emission of a paramagnon.

Second, we propose that the transient T_c enhancement occurs because, in the process of promoting quasiparticles into these long-lived triplet excitons, the laser pulse effectively cools down the quasiparticles system. This also explains why the experiment at 300 K [11] still shows a transient increase of reflectivity, even though the optical data cannot be fit by a model for a superconducting state.

Differently from other laser cooling techniques [42], this mechanism relies on the triplet excitons generated by the laser pulse, which effectively act as charge and spin reservoir soaking up entropy from quasiparticles [43].

While compatible with existing data, various aspects and implications of the present theory can be tested against further experiments. For one, the exciton and its spin-triplet nature could be tackled by magnetic fields and other spectroscopic tools, including e.g., detection of phosphorescence in pumped Cs_3C_{60}.

The possible existence and detection at ambient pressure of the same broad IR absorption peak near 50 meV in the Mott insulating A15-Cs_3C_{60} at ambient pressure would provide support to our proposal of a light-induced intra-molecular exciton ${}^4A_g$ without charge transfer among nearby molecules as opposed to the alternative ${}^4A_u$, a term which besides spin is also parity forbidden and thus much weaker as it requires additional inter-molecular excitations. It may be noted, on the other hand, that the lack of inversion symmetry in merohedrally disordered fcc fullerides might partly allow the parity forbidden dipole transitions [21, 23], mixing in case the spin-quartet ${}^4A_u$ state with the ${}^4A_g$. Our theory of pumping-induced cooling is sufficiently general and would apply to that case too.

Also important would be a re-examination of NMR data, where signatures of a 75 meV spin-gap in Rb_3C_{60} [44] have been so far attributed to thermal population of the ${}^4A_u$ state, for the possible presence of another, possibly even lower energy ${}^4A_g$ spin-quartet state.

Finally, the role of the triplet exciton in the IR-pumping enhancement of T_c could be addressed in a variety of ways and of materials. The strongest candidate remains pressurised Cs_3C_{60}, which met-

allizes and superconducts above 5 kbar, and where the full range of parameters becomes available as a function of pressure. The ideal maximum equilibrium T_c=38 K of fullerides being achieved near 7 kbar[9], it would be exciting to explore whether the transient T_c might conceivably even be raised closer to room temperature.

Acknowledgments

We are very grateful to A. Cavalleri, L. F. Chibotaru, M. Capone, and A. Cantaluppi for comments and discussions, and to S.S. Naghavi for his help. We also acknowledge discussions with A. Isidori, M. Kim and G. Mazza. This work was supported by the European Union, under ERC FIRSTORM, contract N. 692670, ERC MODPHYSFRICT, contract N. 320796, and ERC QMAC, contract N. 319286.

[1] Gunnarsson, O. Superconductivity in fullerides. *Rev. Mod. Phys.* **69**, 575–606 (1997). URL `https://link.aps.org/doi/10.1103/RevModPhys.69.575`.

[2] Capone, M., Fabrizio, M., Castellani, C. & Tosatti, E. Strongly correlated superconductivity. *Science* **296**, 2364–2366 (2002). URL `http://science.sciencemag.org/content/296/5577/2364`. http://science.sciencemag.org/content/296/5577/2364.full.pdf.

[3] Capone, M., Fabrizio, M., Castellani, C. & Tosatti, E. *Colloquium* : Modeling the unconventional superconducting properties of expanded A_3C_{60} fullerides. *Rev. Mod. Phys.* **81**, 943–958 (2009). URL `http://link.aps.org/doi/10.1103/RevModPhys.81.943`.

[4] Fabrizio, M. & Tosatti, E. Nonmagnetic molecular jahn-teller mott insulators. *Phys. Rev. B* **55**, 13465–13472 (1997). URL `http://link.aps.org/doi/10.1103/PhysRevB.55.13465`.

[5] Durand, P., Darling, G. R., Dubitsky, Y., Zaopo, A. & Rosseinsky, M. J. The mott-hubbard insulating state and orbital degeneracy in the superconducting c603- fulleride family. *Nat Mater* **2**, 605–610 (2003). URL `http://dx.doi.org/10.1038/nmat953`.

[6] Kitano, H. *et al.* Evidence for insulating behavior in the electric conduction of $(\mathrm{nh}_3)K_3C_{60}$ systems. *Phys. Rev. Lett.* **88**, 096401 (2002). URL `http://link.aps.org/doi/10.1103/PhysRevLett.88.096401`.

[7] Klupp, G. *et al.* Dynamic jahn–teller effect in the parent insulating state of the molecular superconductor cs3c60. *Nature Communications* **3**, 912 EP – (2012). URL `http://dx.doi.org/10.1038/ncomms1910`.

[8] Micnas, R., Ranninger, J. & Robaszkiewicz, S. Superconductivity in narrow-band systems with local nonretarded attractive interactions. *Rev. Mod. Phys.* **62**, 113–171 (1990). URL `http://link.aps.`

org/doi/10.1103/RevModPhys.62.113.

[9] Ganin, A. Y. *et al.* Bulk superconductivity at 38[thinsp]k in a molecular system. *Nat Mater* **7**, 367–371 (2008). URL http://dx.doi.org/10.1038/nmat2179.

[10] Alloul, H. *et al.* Nmr investigation of the pressure induced mott transition to superconductivity in cs 3 c 60 isomeric compounds. *Journal of Physics: Conference Series* **449**, 012030 (2013). URL http://stacks.iop.org/1742-6596/449/i=1/a=012030.

[11] Mitrano, M. *et al.* Possible light-induced superconductivity in k3c60 at high temperature. *Nature* **530**, 461–464 (2016). URL http://dx.doi.org/10.1038/nature16522.

[12] Sentef, M. A., Kemper, A. F., Georges, A. & Kollath, C. Theory of light-enhanced phonon-mediated superconductivity. *Phys. Rev. B* **93**, 144506 (2016). URL http://link.aps.org/doi/10.1103/PhysRevB.93.144506.

[13] Knap, M., Babadi, M., Refael, G., Martin, I. & Demler, E. Dynamical cooper pairing in nonequilibrium electron-phonon systems. *Phys. Rev. B* **94**, 214504 (2016). URL http://link.aps.org/doi/10.1103/PhysRevB.94.214504.

[14] Kim, M. *et al.* Enhancing superconductivity in A_3c_{60} fullerides. *Phys. Rev. B* **94**, 155152 (2016). URL https://link.aps.org/doi/10.1103/PhysRevB.94.155152.

[15] Kennes, D. M., Wilnel, E. Y., Reichman, D. R. & Millis, A. J. Electronic squeezing of pumped phonons: Negative u and transient superconductivity (2016). ArXiv:1609.03802.

[16] Mazza, G. & Georges, A. Non-equilibrium superconductivity in driven alkali-doped fullerides (2017). ArXiv:1702.04675.

[17] Martin, M. C., Koller, D. & Mihaly, L. *In situ* infrared transmission study of rb- and k-doped fullerenes. *Phys. Rev. B* **47**, 14607–14610 (1993). URL http://link.aps.org/doi/10.1103/PhysRevB.47.14607.

[18] Degiorgi, L. *et al.* Optical properties of the alkali-metal-doped superconducting fullerenes: k_3c_{60} and rb_3c_{60}. *Phys. Rev. B* **49**, 7012–7025 (1994). URL http://link.aps.org/doi/10.1103/PhysRevB.49.7012.

[19] Degiorgi, L. Fullerenes and carbon derivatives: From insulators to superconductors. *Advances in Physics* **47**, 207–316 (1998). URL http://dx.doi.org/10.1080/000187398243555. http://dx.doi.org/10.1080/000187398243555.

[20] Gelfand, M. P. & Lu, J. P. Orientational correlations and order in a3c60. *Applied Physics A* **56**, 215–217 (1993). URL http://dx.doi.org/10.1007/BF00539477.

[21] Deshpande, M. S., Mele, E. J., Rice, M. J. & Choi, H.-Y. Midinfrared conductivity in orientationally disordered doped fullerides. *Phys. Rev. B* **50**, 6993–7006 (1994). URL https://link.aps.org/doi/10.1103/PhysRevB.50.6993.

[22] van den Brink, J., Gunnarsson, O. & Eyert, V. Optical conductivity in A_3c_{60} (A = K,rb). *Phys. Rev. B* **57**, 2163–2167 (1998). URL https://link.aps.org/doi/10.1103/PhysRevB.57.2163.

[23] Chibotaru, L. F. & Ceulemans, A. Symmetry breaking and the band structure of fullerides: the

concomitant role of jahn-teller interactions and electron correlation. In Bevilacqua, G., Martinelli, L. & Terzi, N. (eds.) *Proceedings of the XIV International Symposium on Electron-phonon dynamics and Jahn-Teller effect*, 233–240 (World Scientific, Singapore, 1999).

[24] Auerbach, A., Manini, N. & Tosatti, E. Electron-vibron interactions in charged fullerenes. i. berry phases. *Phys. Rev. B* **49**, 12998–13007 (1994). URL http://link.aps.org/doi/10.1103/PhysRevB.49.12998.

[25] Auerbach, A., Manini, N. & Tosatti, E. Electron-vibron interactions in charged fullerenes. i. berry phases. *Phys. Rev. B* **49**, 12998–13007 (1994). URL http://link.aps.org/doi/10.1103/PhysRevB.49.12998.

[26] O'Brien, M. C. M. Vibronic energies in $c_{60}{}^{n-}$ and the jahn-teller effect. *Phys. Rev. B* **53**, 3775–3789 (1996). URL http://link.aps.org/doi/10.1103/PhysRevB.53.3775.

[27] Dunn, J. L. & Li, H. Jahn-teller effects in the fullerene anion c_{60}^{3-}. *Phys. Rev. B* **71**, 115411 (2005). URL http://link.aps.org/doi/10.1103/PhysRevB.71.115411.

[28] Wehrli, S. & Sigrist, M. Jahn-teller effect versus hund's rule coupling in c_{60}^{N-}. *Phys. Rev. B* **76**, 125419 (2007). URL http://link.aps.org/doi/10.1103/PhysRevB.76.125419.

[29] Naghavi, S. S., Fabrizio, M., Qin, T. & Tosatti, E. Nanoscale orbital excitations and the infrared spectrum of a molecular mott insulator: A15-cs3c60. *Nanoscale* **8**, 17483–17488 (2016). URL http://dx.doi.org/10.1039/C6NR05725J.

[30] Nikolaev, A. V. & Michel, K. H. Molecular terms, magnetic moments, and optical transitions of molecular ions $C_{60}^{m\pm}$. *The Journal of Chemical Physics* **117**, 4761–4776 (2002). URL http://dx.doi.org/10.1063/1.1497644. http://dx.doi.org/10.1063/1.1497644.

[31] Negri, F., Orlandi, G. & Zerbetto, F. Low-lying electronic excited states of buckminsterfullerene anions. *Journal of the American Chemical Society* **114**, 2909–2913 (1992). URL http://dx.doi.org/10.1021/ja00034a023. Found by a multi-configuration interaction method an even larger decrease of $\left(t_{1u}\right)^2\left(t_{1g}\right)^1$ configurations, so large that the lowest is only 100 meV above the ${}^4A_u$ ground state., http://dx.doi.org/10.1021/ja00034a023.

[32] Rai, R. $(\mathrm{T_{1u}} + \mathrm{T_{1g}}) \otimes (\mathrm{h_g} + \tau_{1\mathrm{u}})$ vibronic interaction and superconductivity in C_{60}^{n-} fullerides. *Z. Phys. B* **99**, 327–332 (1996).

[33] Ceulemans, A. & Chibotaru, L. F. Icosahedral $t_{1u}+t_{1g}$ jahn-teller problem. *Phys. Rev. B* **53**, 2460–2462 (1996). URL http://link.aps.org/doi/10.1103/PhysRevB.53.2460.

[34] Iwahara, N., Sato, T., Tanaka, K. & Chibotaru, L. F. Vibronic coupling in C_{60}^- anion revisited: Derivations from photoelectron spectra and dft calculations. *Phys. Rev. B* **82**, 245409 (2010). URL http://link.aps.org/doi/10.1103/PhysRevB.82.245409.

[35] Gunnarsson, O. *et al.* Photoemission spectra of C_{60}^-: Electron-phonon coupling, jahn-teller effect, and superconductivity in the fullerides. *Phys. Rev. Lett.* **74**, 1875–1878 (1995). URL https://link.aps.org/doi/10.1103/PhysRevLett.74.1875.

[36] Hands, I. D. *et al.* Vibronic interactions in the visible and near-infrared spectra of c_{60}^- anions. *Phys.*

Rev. B **77**, 115445 (2008). URL http://link.aps.org/doi/10.1103/PhysRevB.77.115445.

[37] Alqannas, H. S., Lakin, A. J., Farrow, J. A. & Dunn, J. L. Interplay between coulomb and jahn-teller effects in icosahedral systems with triplet electronic states coupled to *h*-type vibrations. *Phys. Rev. B* **88**, 165430 (2013). URL http://link.aps.org/doi/10.1103/PhysRevB.88.165430.

[38] Green, W. H. *et al.* Electronic structures and geometries of c60 anions via density functional calculations. *The Journal of Physical Chemistry* **100**, 14892–14898 (1996). URL http://dx.doi.org/10.1021/jp960689n. http://dx.doi.org/10.1021/jp960689n.

[39] Gunnarsson, O. & Zwicknagl, G. Coulomb pseudopotential, screening and superconductivity in c_{60}. *Phys. Rev. Lett.* **69**, 957–960 (1992). URL http://link.aps.org/doi/10.1103/PhysRevLett.69.957.

[40] Manini, N. & Tosatti, E. Exact zero-point energy shift in the $e \bigotimes$(nE), $t \bigotimes$(nH) many-modes dynamic Jahn-Teller systems at strong coupling. *Phys. Rev. B* **58**, 782–790 (1998). URL http://link.aps.org/doi/10.1103/PhysRevB.58.782.

[41] Rice, M. J. & Choi, H.-Y. Charged-phonon absorption in doped c_{60}. *Phys. Rev. B* **45**, 10173–10176 (1992). URL http://link.aps.org/doi/10.1103/PhysRevB.45.10173.

[42] Ketterle, W. & N.J., V. D. Evaporative cooling of trapped atoms. *Advances in Atomic, Molecular, and Optical Physics* **37**, 181–236 (1996). URL http://www.sciencedirect.com/science/article/pii/S1049250X08601019.

[43] Bernier, J.-S. *et al.* Cooling fermionic atoms in optical lattices by shaping the confinement. *Phys. Rev. A* **79**, 061601 (2009). URL https://link.aps.org/doi/10.1103/PhysRevA.79.061601. Propose a cooling mechanism whose physical principle is close to ours, though in a different context.

[44] Brouet, V., Alloul, H., Garaj, S. & Forró, L. Persistence of molecular excitations in metallic fullerides and their role in a possible metal to insulator transition at high temperatures. *Phys. Rev. B* **66**, 155124 (2002). URL http://link.aps.org/doi/10.1103/PhysRevB.66.155124.

arXiv:1704.05613v1 [cond-mat.str-el] 19 Apr 2017

Supplementary Notes

In these Supplementary Notes we present in detail the calculations whose results are discussed in the main text, as well as other related ones.

S1 LUMO and LUMO+1

The electrons hopping between the sixty carbon atoms of each buckminsterfullerene can be also regarded as moving on a sphere and subject to an icosahedral crystal field. Their wavefunctions are therefore product of a radial one times a combination of spherical harmonics[1]. In particular, upon defining the real spherical harmonics for $m > 0$,

$$\begin{aligned} Y^c_{lm} &= \frac{1}{\sqrt{2}}\left(Y_{lm} + (-1)^m Y_{l-m}\right), \\ Y^s_{lm} &= -\frac{i}{\sqrt{2}}\left(Y_{lm} - (-1)^m Y_{l-m}\right), \end{aligned} \tag{S1.1}$$

then the angular part of the t_{1u} LUMO is

$$\begin{aligned} \psi_z(t_{1u}) &= -\sqrt{\frac{36}{50}}\, Y_{50} - \sqrt{\frac{14}{50}}\, Y^c_{55}, \\ \psi_x(t_{1u}) &= \sqrt{\frac{3}{10}}\, Y^c_{51} - \sqrt{\frac{7}{10}}\, Y^c_{54}, \\ \psi_y(t_{1u}) &= \sqrt{\frac{3}{10}}\, Y^s_{51} + \sqrt{\frac{7}{10}}\, Y^s_{54}, \end{aligned} \tag{S1.2}$$

while that of the t_{1g} LUMO+1 reads

$$\begin{aligned} \psi_z(t_{1g}) &= -Y^s_{65}, \\ \psi_x(t_{1g}) &= \sqrt{\frac{33}{50}}\, Y^s_{61} + \sqrt{\frac{11}{50}}\, Y^s_{64} + \sqrt{\frac{6}{50}}\, Y^s_{66}, \\ \psi_y(t_{1g}) &= -\sqrt{\frac{33}{50}}\, Y^c_{61} + \sqrt{\frac{11}{50}}\, Y^c_{64} - \sqrt{\frac{6}{50}}\, Y^c_{66}. \end{aligned} \tag{S1.3}$$

These sets of orbitals can be regarded for all purposes as p-orbitals. We can also rotate the basis into that of eigenstates of the z-component of the $l = 1$ angular momentum,

$$\begin{aligned} \psi_0 &= \psi_z, \\ \psi_{+1} &= \frac{1}{\sqrt{2}}\left(\psi_x + i\psi_y\right), \\ \psi_{-1} &= -\frac{1}{\sqrt{2}}\left(\psi_x - i\psi_y\right). \end{aligned} \tag{S1.4}$$

In what follows we shall use either equivalent representations. Through equations (S1.2) and (S1.3) one can easily calculate the angular components of the quadrupole moment Q_u and Q_g of the LUMO and LUMO+1, respectively. They have opposite sign and, specifically,

$$\frac{Q_g}{Q_u} \simeq -2.6. \tag{S1.5}$$

This suggests that the vibronic coupling constants between the H_g modes and the t_{1g} electrons have also opposite sign with respect to those of the t_{1u} electrons, and are presumably bigger in absolute value.

S2 Interaction parameters

The multipole expansion of the Coulomb interaction

$$V(\mathbf{r},\mathbf{r}') = \sum_{lm} v_l(r,r')\,(-1)^m\,Y_{lm}\big(\theta_{\mathbf{r}},\phi_{\mathbf{r}}\big)\,Y_{l-m}\big(\theta_{\mathbf{r}'},\phi_{\mathbf{r}'}\big)\,,$$

projected onto the t_{1u}–t_{1g} manifold contains, besides the $l=0$ monopole, i.e. the Slater integral F_0 that is simply the Hubbard U, an exchange H_{exchange}, which includes all $l>0$ terms and, implicitly assuming normal ordering, can be generally written as

$$\begin{aligned}
H_{\text{exchange}} =& \frac{g_1}{2}\left[\frac{4}{3}\sum_a n_{u\,a}\,n_{u\,a} - \frac{2}{3}\sum_{a\neq b} n_{u\,a}\,n_{u\,b} + \sum_{a>b}\Delta_{u\,ab}\,\Delta_{u\,ab}\right] \\
&+ \frac{g_2}{2}\left[\frac{4}{3}\sum_a n_{g\,a}\,n_{g\,a} - \frac{2}{3}\sum_{a\neq b} n_{g\,a}\,n_{g\,b} + \sum_{a>b}\Delta_{g\,ab}\,\Delta_{g\,ab}\right] \\
&+ g_3\left[\frac{4}{3}\sum_a n_{u\,a}\,n_{g\,a} - \frac{2}{3}\sum_{a\neq b} n_{u\,a}\,n_{g\,b} + \sum_{a>b}\Delta_{u\,ab}\,\Delta_{g\,ab}\right] \\
&+ \frac{g_4}{2}\,n_u\,n_u + \frac{g_5}{2}\,n_g\,n_g + g_6\,n_u\,n_g \\
&+ \frac{g_7}{2}\sum_{ab}\left[\Big(\Gamma_{ab}-\Gamma_{ba}\Big)\Big(\Gamma_{ab}-\Gamma_{ba}\Big)\right], \\
&+ \frac{g_8}{2}\sum_{ab}\left[\Big(\Gamma_{ab}+\Gamma_{ba}\Big)\Big(\Gamma_{ab}+\Gamma_{ba}\Big)\right] + \frac{g_9}{2}\sum_{ab}\Gamma_{aa}\,\Gamma_{bb} \\
&\equiv \sum_{i=1}^{9} H_i\,,
\end{aligned} \tag{S2.1}$$

	II	III
g_1	99.4	95.2
g_2	153.6	149.0
g_3	-77.2	-75.0
g_4	43.7	41.7
g_5	34.3	33.7
g_6	24.7	24.7
g_7	227.9	224.7
g_8	26.3	25.0
g_9	-35	-33.5

	II	III
g'_7	-724.89	-710.44
g'_8	438.17	432.83
g'_9	-368.17	-365.83

Table S2.1: Interaction parameters in meV extracted from models II and III of Ref. [2].

where $n_{u\,a}$ and $n_{g\,a}$ are the occupation numbers of orbital $a = x, y, z$ of the t_{1u} LUMO and t_{1g} LUMO+1, respectively, $n_{u(g)} = \sum_a n_{u(g)\,a}$, while

$$\begin{aligned}
\Delta_{u\,ab} &= \sum_\sigma \left(c^\dagger_{u\,a\sigma}\, c_{u\,b\sigma} + H.c. \right), \\
\Delta_{g\,ab} &= \sum_\sigma \left(c^\dagger_{g\,a\sigma}\, c_{g\,b\sigma} + H.c. \right), \\
\Gamma_{ab} &= \sum_\sigma \left(c^\dagger_{u\,a\sigma}\, c_{g\,b\sigma} + H.c. \right),
\end{aligned}$$

with $c^\dagger_{u(g)\,a\sigma}$ and $c_{u(g)\,a\sigma}$ the operators that create and annihilate, respectively, an electron with spin σ and orbital index a in the $t_{1u(g)}$. We mention that g_1, g_2 and g_3 are the coupling constants of the t_{1u}-t_{1u}, t_{1g}-t_{1g} and t_{1u}-t_{1g} quadrupole-quadrupole interactions; while g_7 the coupling constant of the dipole-dipole interaction. In Table S2.1 we list the values of the g_i's extracted by models II and III of Ref. [2].

We note that the Coulomb exchange (S2.1) includes a pair-hopping from t_{1u} to t_{1g} and viceversa. Since the single particle energy of LUMO+1 lies $\Delta\epsilon \gtrsim 1.2$ eV above that of LUMO, we can safely neglect pair-hopping in the calculation of molecular terms. In this approximation and since the t_{1u} and t_{1g} orbitals behave as p-orbitals, we can exploit $O(3)$ symmetry. Therefore each state within the $\left(t_{1u}\right)^n$ subspace can be labelled by a total angular momentum L_u and its z-component Λ_u, as well as by the total spin S_u and its z-component Σ_u. Seemingly a state within the $\left(t_{1g}\right)^m$ subspace can be labelled by L_g, Λ_g, S_g and Σ_g. It follows that a state in the

$\left(t_{1u}\right)^n \otimes \left(t_{1g}\right)^m$ manifold can be labelled by total L, Λ, S and Σ and defined as

$$\begin{aligned} \mid L, \Lambda,\, S, \Sigma; \big(n, L_u, S_u\big), \big(m, L_g, S_g\big)\big\rangle = \sum_{\Lambda_u, \Lambda_g, \Sigma_u, \Sigma_g} C^{L\Lambda}_{L_g\Lambda_g\,, L_u\Lambda_u}\, C^{S\Sigma}_{S_g\Sigma_g\,, S_u\Sigma_u} \\ \mid m,\, L_g, \Lambda_g,\, S_g, \Sigma_g\big\rangle \;\mid n,\, L_u, \Lambda_u,\, S_u, \Sigma_u\big\rangle\,, \end{aligned} \tag{S2.2}$$

where $C^{ab}_{cd,ef}$ are Clebsch-Gordan coefficients. The matrix elements of the exchange Hamiltonian, which is a scalar under $O(3)$, can be readily calculated by means of the Wigner-Eckart theorem. In reality, it is convenient to manipulate H_{exchange} and make it more manageable through the Wigner-Eckart theorem. We define the quadrupole operators

$$Q_{2m} = \sqrt{\frac{20\,\pi}{3}}\; Y_{2m}\,,$$

with $m = -2, \ldots, 2$, for both t_{1u} and t_{1g} electrons. Using the complex representation (S1.4), so that the orbitals are now labeled by the projection of the $l = 1$ angular momentum, i.e. $a = -1, \ldots, 1$, the $m = 0$ component of the quadrupole is

$$Q_{p\,20} = \frac{1}{\sqrt{3}}\Big(2n_{p\,0} - n_{p\,+1} - n_{p\,-1}\Big)\,, \tag{S2.3}$$

where $p = u, g$ refers to t_{1u} and t_{1g} electrons. One can readily show that, upon transformation into the complex representation (S1.4), the following equivalence holds

$$\begin{aligned} &\frac{4}{3}\sum_a n_{p\,a}\, n_{p\,a} - \frac{2}{3}\sum_{a\neq b} n_{p\,a}\, n_{p\,b} + \sum_{a>b} \Delta_{p\,ab}\, \Delta_{p\,ab} \;\longrightarrow\; \sum_m (-1)^m\, Q_{p\,2m}\, Q_{p\,2-m} \\ &\equiv \mathbb{Q}_{2p}\cdot\mathbb{Q}^\dagger_{2p} = 15 - 4S_p\Big(S_p+1\Big) - L_p\Big(L_p+1\Big) - \frac{5}{3}\Big(n_p - 3\Big)^2\,, \end{aligned} \tag{S2.4}$$

where the dot represents the scalar product between vector spherical harmonics, and the last expression is the value on a state identified by n_p electrons in the t_{1p} orbital, $p = u, g$, with total angular momentum L_p and spin S_p.
Moreover the sum of operators in Eq. (S2.1) that involve the coupling constants g_7, g_8 and g_9 can be equivalently written, once pair hopping terms are neglected, as

$$\begin{aligned} \sum_{i=7}^{9} H_i =& g'_7\left(\mathbf{S}_u\cdot\mathbf{S}_g + \frac{1}{4}\,n_u\,n_g\right) + g'_8\left(\mathbb{Q}^\dagger_{2g}\otimes\mathbf{S}_g\cdot\mathbb{Q}_{2u}\otimes\mathbf{S}_u + \frac{1}{4}\,\mathbb{Q}^\dagger_{2g}\cdot\mathbb{Q}_{2u}\right) \\ &+ g'_9\left(\mathbf{L}_g\otimes\mathbf{S}_g\cdot\mathbf{L}_u\otimes\mathbf{S}_u + \frac{1}{4}\,\mathbf{L}_u\cdot\mathbf{L}_g\right), \end{aligned} \tag{S2.5}$$

where e.g. $\mathbf{L}_u \otimes \mathbf{S}_u$ is the single-particle spin-orbit operator for t_{1u} electrons that corresponds to an orbital operator with $l = 1$ and a spin operator with $s = 1$. Seemingly $\mathbb{Q}_{2u} \otimes \mathbf{S}_u$ is a single-particle operator with orbital momentum $l = 2$ and spin $s = 1$. The new coupling constants are defined in terms of those in Table S2.1 through

$$\begin{aligned} g_7' &= -\frac{8}{3}\, g_7 - \frac{16}{3}\, g_8 + \frac{2}{3}\, g_9 \,, \\ g_8' &= 2g_7 - 2g_8 + g_9 \,, \\ g_9' &= -2g_7 + 2g_8 + g_9 \,, \end{aligned} \tag{S2.6}$$

and their values are shown in the same table.
In conclusion the exchange Hamiltonian (S2.1) without pair hopping terms among t_{1u} and t_{1g} can be rewritten as

$$\begin{aligned} H_{\text{exchange}} = {} & \frac{g_1}{2}\left[15 - 4S_u\Big(S_u+1\Big) - L_u\left(L_u+1\right) - \frac{5}{3}\left(n_u-3\right)^2\right] \\ & + \frac{g_2}{2}\left[15 - 4S_g\Big(S_g+1\Big) - L_g\left(L_g+1\right) - \frac{5}{3}\left(n_g-3\right)^2\right] + g_3\, \mathbb{Q}_{2g}^\dagger \cdot \mathbb{Q}_{2u} \\ & + \frac{g_4}{2}\, n_u\, n_u + \frac{g_5}{2}\, n_g\, n_g + g_6\, n_u\, n_g \\ & + g_7'\left(\mathbf{S}_u \cdot \mathbf{S}_g + \frac{1}{4}\, n_u\, n_g\right) + g_8'\left(\mathbb{Q}_{2g}^\dagger \otimes \mathbf{S}_g \cdot \mathbb{Q}_{2u} \otimes \mathbf{S}_u + \frac{1}{4}\, \mathbb{Q}_{2g}^\dagger \cdot \mathbb{Q}_{2u}\right) \\ & + g_9'\left(\mathbf{L}_g \otimes \mathbf{S}_g \cdot \mathbf{L}_u \otimes \mathbf{S}_u + \frac{1}{4}\, \mathbf{L}_u \cdot \mathbf{L}_g\right), \end{aligned} \tag{S2.7}$$

which is easier to deal with by means of Wigner-Eckart theorem, and reproduces all molecular terms obtained in Ref. [2].
For our purposes, we shall concentrate here only on few configurations. Within the $\left(t_{1u}\right)^3$ subspace, we consider all twenty states, i.e. the multiplets with $L = 0$ and $S = 3/2$, $L = 2$ and $S = 1/2$, and finally $L = 1$ and $S = 1/2$, which we denote as ${}^4A_u$, ${}^2H_u$ and ${}^2T_{1u}$, respectively. On the contrary, within the $\left(t_{1u}\right)^2\left(t_{1g}\right)^1$ subspace, we shall focus only on the states with $L = 2$ and $S = 3/2$, and $L = 0$ and $S = 3/2$, which we denote as ${}^4H_g$ and ${}^4A_g$, respectively. Their energies are explicitly

$$\begin{aligned} E\Big({}^4A_u\Big) &= -5g_1 + 3g_4 \,, \\ E\Big({}^2H_u\Big) &= -2g_1 + 3g_4 \,, \\ E\Big({}^2T_{1u}\Big) &= 3g_4 \,, \\ E\Big({}^4H_g\Big) &= \Delta\epsilon - \frac{5}{3}\, g_1 - \frac{1}{3}\, g_3 + g_4 + 2\, g_6 + g_7' - \frac{1}{6}\, g_8' + \frac{1}{2}\, g_9' \,, \\ E\Big({}^4A_g\Big) &= \Delta\epsilon - \frac{5}{3}\, g_1 - \frac{10}{3}\, g_3 + g_4 + 2\, g_6 + g_7' - \frac{5}{3}\, g_8' - g_9' \,, \end{aligned} \tag{S2.8}$$

	g	ω(meV)	$E_{\rm JT} = \omega\, g^2/2$ (meV)	$3E_{\rm JT}/2$ (meV)
(1)	1.14	100.15	64.83	97.25
(2)	1.12	99.89	62.38	93.56
(3)	1.01	96.61	57.62	86.43
(4)	1.43	76.61	78.25	117.37
(5)	1.41	82.84	82.00	123.00

Table S3.1: Dimensionless vibronic coupling g, phonon frequency ω and Jahn-Teller energy gain $E_{\rm JT} = \omega\, g^2/2$ obtained in Ref. [4] by fitting two sets of photoemission spectra of C_{60}^-. The labels are the same as in Table I. of [4]. (1), (2) and (3) refer to three equally good fits of the same experimental data, while (4) and (5) to fits of another set of data.

where $\Delta\epsilon$ is the single-particle energy difference between t_{1g} and t_{1u} electrons.

S3 Jahn-Teller effect

The quadrupole moment of the t_{1u} and the t_{1g} electrons are coupled to the eight fivefold degenerate H_g vibrations, which actually correspond to quadrupolar distortions of the molecule. In the single-mode approximation [3] and using the same conventions, we have to add the following operator to the Hamiltonian

$$H_{\rm JT} = \sqrt{\frac{3}{4}}\; g\,\omega \sum_{m=-1}^{1} (-1)^m\, q_{-m} \left(Q_{u\,2m} - \lambda\, Q_{g\,2m} \right) + \frac{\omega}{2} \left(\mathbf{q}\cdot\mathbf{q}^\dagger + \mathbf{p}\cdot\mathbf{p}^\dagger \right), \qquad \text{(S3.1)}$$

where, as mentioned previously, $\lambda \geq 1$. There are different estimates of g and ω. In Table S3.1 we list the results of Ref. [4] obtained by fitting photoemission spectra of C_{60}^-.

S3.1 Anti-adiabatic regime

The simplest approximation of the Jahn-Teller Hamiltonian (S3.1) is to integrate out the vibrations and neglect the frequency dependence of the vibron-mediated interaction. This corresponds to the so-called anti-adiabatic approximation [5], and amounts to an additional exchange interaction

$$\delta H_{\rm exchange} = -\frac{3}{4}\, E_{\rm JT} \left(\mathbb{Q}^\dagger_{u\,2} - \lambda\, \mathbb{Q}^\dagger_{g\,2} \right) \cdot \left(\mathbb{Q}_{u\,2} - \lambda\, \mathbb{Q}_{g\,2} \right), \qquad \text{(S3.2)}$$

which, unlike Eq. (S2.7), must not be normal ordered, so that

$$\delta H_{\rm exchange} = :\delta H_{\rm exchange}: - \frac{5}{2}\, E_{\rm JT} \left(n_u + \lambda^2\, n_g \right), \qquad \text{(S3.3)}$$

where : (...) : denotes normal ordering. This implies that the coupling constants g_1, g_2 and g_3 changes according to

$$\begin{aligned} g_1 &\to g_{1*} = g_1 - \frac{3}{2}\, E_{\rm JT}\,, \\ g_2 &\to g_{2*} = g_2 - \frac{3}{2}\,\lambda^2\, E_{\rm JT}\,, \\ g_3 &\to g_{3*} = g_3 + \frac{3}{2}\,\lambda\, E_{\rm JT}\,. \end{aligned} \tag{S3.4}$$

Through Eqs. (S2.8) and (S3.3), we can actually define three different spin gaps, $\Delta^{(1)}$, $\Delta^{(2)}$, and $\Delta^{(3)}$,

$$\Delta^{(1)} = E\Big({}^4A_u\Big) - E\Big({}^2T_{1u}\Big) = -5\, g_{1*} = 5\,\Big(\frac{3}{2}\, E_{\rm JT} - g_1\Big) \simeq -476 + \frac{15}{2}\, E_{\rm JT}\,, \tag{S3.5}$$

$$\Delta^{(2)} = E\Big({}^4A_g\Big) - E\Big({}^2T_{1u}\Big) \simeq \Delta\epsilon - 1011 - \frac{5}{2}\, E_{\rm JT}\,\Big(2\lambda + \lambda^2 - 2\Big)\,, \tag{S3.6}$$

$$\Delta^{(3)} = E\Big({}^4H_g\Big) - E\Big({}^2T_{1u}\Big) \simeq \Delta\epsilon - 1135 - \frac{1}{2}\, E_{\rm JT}\Big(\lambda + 5\lambda^2 - 10\Big)\,, \tag{S3.7}$$

where energies are in meV and we use the interaction model III of Table S2.1.

In solution the molecular ground state of C_{60}^{3-} seems to be a spin doublet [6, 7, 8], with a very small excitation energy to another magnetic state [6], which was ascribed to the ${}^2T_{1u}$ splitting into ${}^2E_u$ and ${}^2A_u$ in a non-icosahedral environment, or, alternatively, to an excitation between the spin-doublet ${}^2T_{1u}$ ground state and a spin-quartet with A symmetry [9]. C_{60}^{2-} in solution has instead a non-magnetic ground state with a sizeable spin gap of 75 meV. There are also evidences of a lower magnetic state lying only a wavenumber above the ground state [8], which might correspond to a genuine C_{60}^{2-} spin excitation or, more likely, to the contribution of $C_{120}O^{2-}$ and $C_{120}O^{4-}$ impurities [7].
In the solid state, NMR spectra in metallic A_3C_{60} and non-magnetic insulating A_2C_{60} reveal the existence of a spin gap of magnitude $75-100$ meV [10, 11]. We must however mention that there are discrepancies between the magnetic susceptibility of A_3C_{60} (A=K,Rb) measured, e.g., by ESR and by SQUID, see [12] and references therein. While the former is an increasing function of temperature, the latter decreases with increasing T. This behaviour has been explained assuming the presence of magnetic impurities [12], though it could well indicate the existence of intrinsic low-lying spin excitations.
Electronic structure calculations of isolated molecular anions C_{60}^{n-} [9] find almost vanishing spin gaps between distorted ${}^1A_g$ and ${}^3T_{1g}$ states for $n = 2$, and between undistorted ${}^4A_u$ and distorted ${}^2T_{1u}$ for $n = 3$. However, if one adds for $n = 3$ the zero-point energy of the molecular vibrations [13], the energy balance changes appreciably in favour of the distorted spin-doublet, leading to a $\Delta^{(1)} = 75$ meV, see Eq. (S3.5), much in agreement with the experimental value in

the solid state. This calculation seems therefore to support the original interpretation of EPR spectra of C_{60}^{3-} in solution given by the authors of Ref. [6], who associated the observed low-lying excitation to the ${}^2T_{1g}$ splitting in a non-icosahedral environment. There are so far no calculations of the vibrational zero-point energy contribution in C_{60}^{2-}. However, since both ${}^1A_g$ and ${}^3T_{1g}$ allow for unimodal Jahn-Teller distortion, we expect they will have similar zero-point energy gains and thus remain almost degenerate. Therefore, while electronic structure calculations of isolated molecular anions, including the zero-point energy of the molecular vibrations, seem to reproduce the physics of C_{60}^{3-} both in solution and in the solid state, they might fail in the case of C_{60}^{2-}, where instead the evidence of a low-spin ground state well separated from high-spin excited states is more undeniable, especially in alkali fullerides.

The conventional explanation of this failure invokes the screening of Coulomb exchange by nearby polarisable molecules, which is absent in single molecule calculations. This argument is in our opinion not fully satisfying. First, we mentioned that single molecule calculations for C_{60}^{3-}, including the zero-point energy for vibrations, do predict a spin-doublet ground state with a gap to the spin-quartet state of similar magnitude to that observed in A_3C_{60}. Second, we do not understand why the quadrupole-quadrupole electron-electron interaction should be screened, whereas the interaction between the electron and molecular quadrupoles, of similar origin, should not. We instead tend to believe that electronic structure calculation may rather fail because of correlation effects not well captured by independent particle schemes.

In this perspective, we cannot exclude that the low lying spin excitations observed in C_{60}^{3-} in solutions [6], and by SQUID measurements in K_3C_{60} and Rb_3C_{60}, might actually correspond to a genuine molecular excitation between the spin-doublet ground state and a spin-quartet one, different from the ${}^4A_u$ and elusive to electronic structure calculations because of correlations.

We shall argue that such a state does exist and must be associated to the lowest among $\Delta^{(2)}$ and $\Delta^{(3)}$, i.e. to an excitation between a $\left(t_{1u}\right)^3$ spin-doublet and a $\left(t_{1u}\right)^2\left(t_{1g}\right)^1$ spin-quartet. Under this assumption, $\Delta^{(1)} \simeq 75$ meV implies

$$E_{\rm JT} \gtrsim 74.5 \text{ meV}\,, \tag{S3.8}$$

larger than the estimates (1)–(3) in Table S3.1, but lower than (4) and (5). The magnitudes of $\Delta^{(2)}$ and $\Delta^{(3)}$ critically depend on $\Delta\epsilon$ and λ. Electronic structure calculations [9] suggests that $\lambda \simeq 1.25$. Near IR absorption spectra of C_{60}^- [14, 15] show a main peak at $\Delta\epsilon_* = 1150 - 1163$ meV, which is the bare $t_{1u} \to t_{1g}$ excitation energy $\Delta\epsilon$ reduced by a Jahn-Teller contribution. In the antiadiabatic limit we are using here,

$$\Delta\epsilon_* = \Delta\epsilon - \frac{5}{2}\, E_{\rm JT}\left(\lambda^2 - 1\right), \tag{S3.9}$$

which, through Eq. (S3.8), would imply $\Delta\epsilon = 1253 - 1266$ meV but negative spin gap $\Delta^{(2)}$. This result contradicts the experimental evidence and might be due to the antiadiabatic approximation that overestimates the Jahn-Teller effect, which is stronger in ${}^4A_g$ than in ${}^2T_{1u}$. Since the

antiadiabatic approximation has nonetheless the advantage of being very simple and to depend only on the overall Jahn-Teller energy $E_{\rm JT}$ and not on the precise values of the vibrational coupling constants to each of the eight H_g modes, we shall keep using such an approximation and cure its deficiency by a 14% screening reduction of the Coulomb exchange that leads to the following estimates

$$\begin{aligned} E_{\rm JT} &\simeq 64.6 \text{ meV}\,, \\ \Delta\epsilon &\simeq 1241 - 1254 \text{ meV}\,, \\ \Delta^{(1)} &\simeq 75 \text{ meV}\,, \\ \Delta^{(2)} &\simeq 38 - 51 \text{ meV}\,, \\ \Delta^{(3)} &\simeq 295 - 308 \text{ meV}\,. \end{aligned} \tag{S3.10}$$

S3.2 Variational calculation

In order to assess the accuracy of the antiadiabatic limit, in this section we shall attach the Jahn-Teller problem by a variational approach introduced by Wehrli and Sigrist [16], which we first briefly sketch.
One starts from the wavefunction of a product state,

$$\mid \Psi(\mathbf{q})\big\rangle = \mid \mathbf{q}\rangle_v \otimes \mid \psi(\mathbf{q})\rangle_e\,, \tag{S3.11}$$

where $\mid \mathbf{q}\rangle_v$ is a coherent state of the H_g modes with average displacement $\mathbf{q}$, see Eq. (S3.1), which serves as a variational parameter, while $\mid \psi(\mathbf{q})\rangle_e$ is the (Born-Oppenheimer) electronic ground state at fixed $\mathbf{q}$. Since the Hamiltonian has $SO(3)$ symmetry, its expectation value over a wavefunction like (S3.11) is also invariant under rotation of $\mathbf{q}$. In other words, under the transformation

$$\mathbf{q} = \begin{pmatrix} q_{+2} \\ q_{+1} \\ q_0 \\ q_{-1} \\ q_{-2} \end{pmatrix} \rightarrow \hat{U}(\Theta)\,\mathbf{q} \qquad \mid \Psi(\mathbf{q})\big\rangle \rightarrow \mid \Psi\Big(\hat{U}(\Theta)\,\mathbf{q}\Big)\,\big\rangle\,, \tag{S3.12}$$

where $\hat{U}(\Theta)$ is the $SO(3)$ rotation by Euler angle Θ, in this specific case the Wigner-D matrix with angular momentum $L = 2$, the expectation value of the Hamiltonian is independent of Θ. We can enforce $SO(3)$ symmetry by parametrising the displacement $\mathbf{q}$ through a magnitude q and shape-angle α, as

$$\mathbf{q} = \frac{q}{\sqrt{2}} \begin{pmatrix} \sin\alpha \\ 0 \\ \sqrt{2}\,\cos\alpha \\ 0 \\ \sin\alpha \end{pmatrix}\,,$$

and defining a variational wavefunction

$$\mid \Psi^L_{MK}(q,\alpha) \rangle = \mathcal{Q}^L_{MK} \mid \Psi(\mathbf{q}) \rangle , \tag{S3.13}$$

through the projection operator

$$\mathcal{Q}^L_{MK} = \frac{2L+1}{8\pi^2} \int d\Theta \, D^L_{MK}(\Theta) \, \hat{U}(\Theta)$$

where the integration is over the Euler angles,

$$\int d\Theta = \int_0^{2\pi} d\phi \int_0^{2\pi} d\gamma \int_0^{\pi} \sin\theta \, d\theta ,$$

$D^L_{MK}(\Theta)$ are the real Wigner-D functions and $\hat{U}(\Theta)$ is the rotation operator. The variational wavefunction thus depends on two variational parameters, q and α, as well as on the quantum numbers L, the total angular momentum, its z-component M, and an additional integer K that is non-zero only in the case of bimodal distortions $\sin\alpha \neq 0 \neq \cos\alpha$.
In the case of C_{60}^- with an electron in the t_{1u} orbital, $\alpha = 0$, i.e. the distortion is unimodal, and the variational energy is obtained by minimising with respect to q the functional

$$E\left[(t_{1u})^1\right](g,q) = \left(\frac{q^2}{2} h(q) - gq\right)\omega$$

where

$$h(q) = \frac{\int_{-1}^{1} t^2 \left(\frac{3}{2}t^2 - \frac{1}{2}\right) e^{-\frac{3}{4}q^2(1-t^2)} dt}{\int_{-1}^{1} t^2 e^{-\frac{3}{4}q^2(1-t^2)} dt} .$$

Seemingly, the energies of C_{60}^{3-} in the $S = 1/2$ $\left(t_{1u}\right)^3$ subspace, with bimodal distortion and thus $K \neq 0$, or in the $S = 3/2$ $\left(t_{1u}\right)^2\left(t_{1u}\right)^1$ subspace with unimodal distortion, are obtained by minimising with respect to q the functionals

$$\frac{E\left[(t_{1u})^3\right](g,q)}{\omega} = \text{LowerEigenvalue}\left[\begin{array}{cc} \frac{q^2}{2}\frac{G^T_{L,K}}{N^T_{L,K}} + \frac{r\,E\left({}^2T_{1u}\right)}{\omega} & \frac{\sqrt{3}}{2} gq \frac{N^T_{L,K} + N^H_{L,K}}{\sqrt{N^T_{L,K} N^H_{L,K}}} \\ \frac{\sqrt{3}}{2} gq \frac{N^T_{L,K} + N^H_{L,K}}{\sqrt{N^T_{L,K} N^H_{L,K}}} & \frac{q^2}{2}\frac{G^H_{L,K}}{N^H_{L,K}} + \frac{r\,E\left({}^2H_u\right)}{\omega} \end{array}\right],$$

and

$$\frac{E\left[\left(t_{1u}\right)^{2}\left(t_{1g}\right)^{1}\right](g,q)}{\omega}=\Delta\epsilon$$
$$+\,\text{LowerEigenvalue}\left[\begin{array}{cc}\frac{q^{2}}{2}\frac{F_{L}^{1}}{F_{L}^{0}}+\frac{r\,E\left({}^{4}A_{g}\right)}{\omega} & \frac{\lambda g q}{\sqrt{2}}\left(\sqrt{\frac{F_{L}^{1}}{F_{L}^{0}}}+\sqrt{\frac{F_{L}^{0}}{F_{L}^{1}}}\right)\\ \frac{\lambda g q}{\sqrt{2}}\left(\sqrt{\frac{F_{L}^{1}}{F_{L}^{0}}}+\sqrt{\frac{F_{L}^{0}}{F_{L}^{1}}}\right) & \frac{q^{2}}{2}\frac{F_{L}^{2}}{F_{L}^{1}}-\lambda g q+\frac{r\,E\left({}^{4}H_{g}\right)}{\omega}\end{array}\right],$$

where

$$\begin{aligned}
N_{L,K}^{T}\left(q\right) &= \frac{2L+1}{8\pi^{2}}\int d\Theta\, D_{KK}^{L}(\Theta)\, D_{00}^{1}(\Theta)\, \mathrm{e}^{-\frac{q^{2}}{2}\left(1-D_{22}^{2}(\Theta)\right)}\,,\\
N_{L,K0}^{H}\left(q\right) &= \frac{2L+1}{8\pi^{2}}\int d\Theta\, D_{KK}^{L}(\Theta)\, D_{-2-2}^{2}(\Theta)\, \mathrm{e}^{-\frac{q^{2}}{2}\left(1-D_{22}^{2}(\Theta)\right)}\,,\\
G_{L,K}^{T}\left(q\right) &= \frac{2L+1}{8\pi^{2}}\int d\Theta\, D_{KK}^{L}(\Theta)\, D_{00}^{1}(\Theta)\, D_{22}^{2}(\Theta)\, \mathrm{e}^{-\frac{q^{2}}{2}\left(1-D_{22}^{2}(\Theta)\right)}\,,\\
G_{L,K}^{H}\left(q\right) &= \frac{2L+1}{8\pi^{2}}\int d\Theta\, D_{KK}^{L}(\Theta)\, D_{-2-2}^{2}(\Theta)\, D_{22}^{2}(\Theta)\, \mathrm{e}^{-\frac{q^{2}}{2}\left(1-D_{22}^{2}(\Theta)\right)}\,,\\
F_{L}^{n}\left(q\right) &= \frac{2L+1}{2}\int_{-1}^{1} dt\, P_{L}\left(t\right)\,\left(P_{2}\left(t\right)\right)^{n}\,\mathrm{e}^{-\frac{3}{2}q^{2}\left(1-t^{2}\right)}\,, \qquad \text{(S3.14)}
\end{aligned}$$

involve real Wigner-D functions and Legendre Polynomials. The lower energies are obtained for $(L,K)=(1,0)\,,(2,-2)$, and for $L=0,2$ in the $\left(t_{1u}\right)^{3}$ and $\left(t_{1u}\right)^{2}\left(t_{1g}\right)^{1}$ cases, respectively.
We have optimised the wavefunctions for two vibrational frequencies in the single-mode approximation, rows (1) and (4) in Table S3.1. The value of $\Delta\epsilon$ is obtained as before through the main near-IR absorption peak $\Delta\epsilon_{*}=1150-1163$ meV subtracting the Jahn-Teller contribution. In the variational scheme the latter can be approximately obtained through the product state (S3.11) assuming a vertical Franck-Condon transition, which provides a somehow lower estimate $\Delta\epsilon\simeq 1080$ meV. We observe that the two different vibrational frequencies lead to similar results when plotted as function of the Jahn-Teller energy. Moreover, consistently with the Jahn-Teller effect being overestimated within the anti-adiabatic approximation, in this variational approach we get sensible results only assuming a larger screening reduction, $r=0.78$ of the bottom panels, and larger Jahn-Teller energy $E_{\mathrm{JT}}\sim 90$ meV. Such a value is above the estimates extracted from most recent photoemission data, (1)–(3) in Table S3.1, but close to those usually adopted in the literature, see e.g. [16]. Moreover, as suggested in Refs. [17, 18], quadratic couplings among the electrons and H_g modes, allowed since $H_g\times H_g$ includes still H_g and not accounted for in the fit, might be not negligible. In view of the uncertainty in the values of the vibrational

coupling constants and in the accuracy of the single-mode approximation, in the main text we have preferred to emphasise more the results obtained in the antiadiabatic approximation, which depend on a single vibrational parameter E_{JT}.

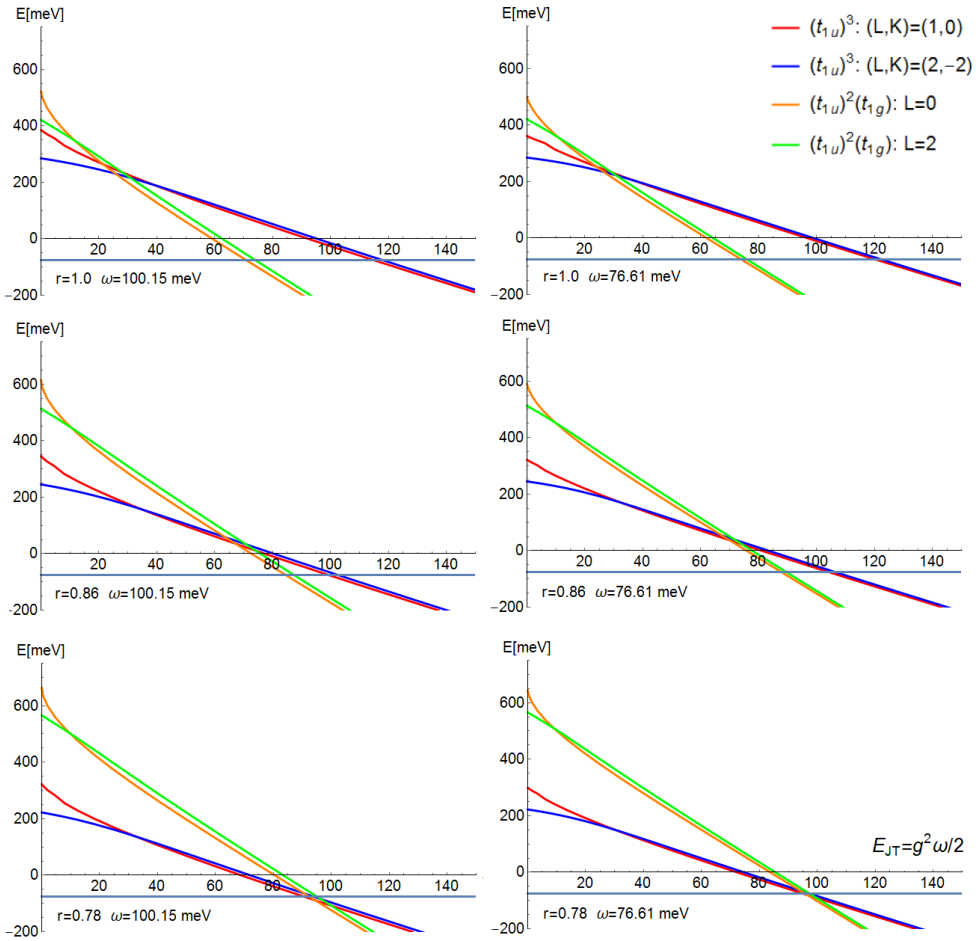

Figure S3.1: Variational energies for the $(t_{1u})^3$ and the $(t_{1u})^2\,(t_{1g})^1$ configurations. Left panels are obtained with $\omega = 100.13$ meV meV while right panels with $\omega = 76.61$ meV. Top panels corresponds to $r = 1$, central panels to $r = 0.86$, and finally bottom panels to $r = 0.78$. The zero of energy is fixed at the energy of the ${}^4A_u$ state, while the horizontal line at $E = -75$ meV is supposedly the energy of the ${}^2T_{1u}$, which corresponds to $(L, K) = (1, 0)$. Seemingly, the state ${}^2H_u$ corresponds to $(L, K) = (2, -2)$, while $L = 0$ and $L = 2$ correspond to the states ${}^4A_g$ and ${}^4H_g$, respectively.

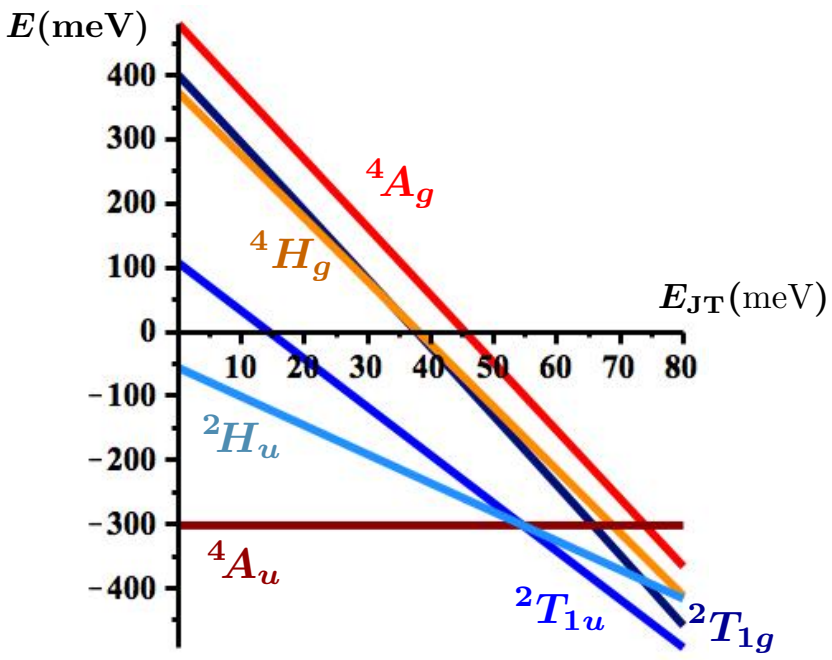

Figure S3.2: Molecular terms calculated in the antiadiabatic approximation, to be compared with Fig. 2(a) of the manuscript. The parameters are the same as in that figure, but replacing Eq. (S3.4) with (S3.15) with $\lambda_2 = 0.1$ and $\lambda_1 = 1.7$. The dark blue line is a $^2T_{1g}$ state pushed by the new parameters that we use close to the $^2T_{1u}$ ground state.

We conclude with some comments concerning the results of the present and the previous sections. Originally we were hoping that, in the presence of Jahn-Teller, the lowest energy state within the $(t_{1u})^2(t_{1g})^1$ subspace should have been one within the manifold of symmetry $^2T_{1g}$, which includes a very low-lying state already in the absence of JT. Evidently that circumstance would have been very pleasant since the $^2T_{1u} \rightarrow^2 T_{1g}$ transition is parity and spin allowed. We mention that the $^2T_{1g}$ manifold comprises three states: a state (1) obtained by the $(t_{1u})^2$ ^1A_g plus one electron in the t_{1g}; a state (2) obtained by the $(t_{1u})^2$ ^1H_g coupled to one electron in the t_{1g} into a $^2T_{1g}$-symmetry state; and finally a state (3) obtained by the $(t_{1u})^2$ $^3T_{1g}$ coupled to one electron in the t_{1g} still into a $^2T_{1g}$-symmetry state. We note that the ^1A_g state within the $(t_{1u})^2$ subspace is the one gaining the largest Jahn-Teller energy. Therefore our expectation was that $^1A_g \oplus (t_{1g})^2 \rightarrow^2 T_{1g}(1)$ should have been the winner among the three. However, the Coulomb exchange splitting couples among each other all the three $^2T_{1g}$ states, more strongly the state (2) with (3). As the result, the lowest $^2T_{1g}$ state in the absence of JT is a mixture with almost similar weights of (2) and (3) and none of (1). The next, 1 eV above, is mostly contributed by (1), and lastly the highest, 2 eV above, is again a mixture mainly of (2) and (3). The Jahn-Teller effect, though sizeable, is not strong enough to push (1) down enough and below the spin-quartet ^4A_g. However there might still be a chance for that to happen under particular circumstances that would need further investigation. It has been suggested [17] that

the t_{1g} electrons may couple preferentially of H_g modes that are instead the less coupled to t_{1u} electrons. If this were confirmed, one should better work in a two-mode approximation, rather than a single-mode. Alternatively, within the anti-adiabatic approximation, the equation (S3.4) should be replaced by

$$\begin{aligned} g_1 &\to g_{1*} = g_1 - \frac{3}{2}\, E_{\rm JT}\,, \\ g_2 &\to g_{2*} = g_2 - \frac{3}{2}\, \lambda_1^2\, E_{\rm JT}\,, \\ g_3 &\to g_{3*} = g_3 + \frac{3}{2}\, \lambda_2\, E_{\rm JT}\,. \end{aligned} \tag{S3.15}$$

with $0 < \lambda_2 \ll \lambda_1$. With properly massaged values of $\lambda_2 = 0.1$ and $\lambda_1 = 1.7$ we obtain the molecular terms of Fig. S3.2, to be compared with Fig. 2(a) of the manuscript. Indeed with such values we are able to push ${}^2T_{1g}$ below ${}^4A_g$ and close to the ${}^2T_{1u}$ ground state. As we mentioned, this scenario could explain much more simply the origin of the mid infrared peak. However the cooling mechanism that we propose, see the following section, would not work anymore. One could consider a different scheme taking into account the radiative decay of such an exciton, which would be much faster than that of ${}^4A_g$, and the fact that also the ${}^2T_{1g}$ is entropy-rich. We tend however to believe more in the physical parameters used in the manuscript, mainly because this new scenario requires $\lambda_2 \lesssim 0.1$, which implies that the set of H_g modes that couple to t_{1u} has almost no overlap to that coupling to t_{1g}. Nonetheless we think this alternative possibility worth to be further investigated by more *ab-initio* techniques.

S4 Boltzmann equation and effective temperature

In this section we give some details on the Boltzmann equation that we use to describe the time evolution of the quasiparticle distribution under the effect of the laser pulse. First we make explicit all approximations. We mentioned that the energy supplied by the laser pulse is partly used to create the exciton by absorbing/emitting spin-triplet quasiparticle-quasihole excitations, and partly to emit H_g vibrations because of the Franck-Condon effect. We shall neglect the latter and thus assume a δ-like spectrum of the exciton $\mathcal{A}_{\rm exc}(\epsilon) = \delta\big(\epsilon - E_{\rm exc}\big)$. Within such an approximation, the effect of the laser is therefore: (1) to create excitons and correspondingly lower the density of quasiparticles; (2) change the distribution of spin-triplet quasiparticle-quasihole excitations. The diminishing of quasiparticle density below half-filling already brings about a reduction of quasiparticle entropy. We shall neglect this effect and just concentrate on the distribution of quasiparticle-quasihole excitations, which implies underestimating the entropy reduction. Finally, we shall not take into account the radiative decay of an exciton back into a photon with simultaneous emission/absorption of a spin-triplet quasiparticle-quasihole excitation, as well as non-radiative decay processes.

The equations that control the rate of creation of triplet excitons per molecule, N_{S_z} with $S_z = -1, 0, 1$, are

$$\begin{aligned}
\dot{N}_{+1}(t) &= \gamma \Big(1 - N_{\rm exc}(t)\Big) \sum_{a=1}^{3} \int d\epsilon\, \rho(\epsilon)\, \rho(\epsilon + \Delta\omega)\, n_{a\uparrow}(\epsilon, t)\, \bar{n}_{a\downarrow}\big(\epsilon + \Delta\omega, t\big)\Big)\,, \\
\dot{N}_{-1}(t) &= \gamma \Big(1 - N_{\rm exc}(t)\Big) \sum_{a=1}^{3} \int d\epsilon\, \rho(\epsilon)\, \rho(\epsilon + \Delta\omega)\, n_{a\downarrow}(\epsilon, t)\, \bar{n}_{a\uparrow}\big(\epsilon + \Delta\omega, t\big)\Big)\,, \\
\dot{N}_{0}(t) &= \frac{\gamma}{2} \Big(1 - N_{\rm exc}(t)\Big) \sum_{a=1}^{3} \sum_{\sigma} \int d\epsilon\, \rho(\epsilon)\, \rho(\epsilon + \Delta\omega)\, n_{a\sigma}(\epsilon, t)\, \bar{n}_{a\sigma}\big(\epsilon + \Delta\omega, t\big)\Big)\,,
\end{aligned} \tag{S4.1}$$

where $n_{a\sigma}(\epsilon, t)$ is the distribution of quasiparticles with orbital index a and spin σ, $\bar{n}_{a\sigma}(\epsilon, t) = 1 - n_{a\sigma}(\epsilon, t)$, $\Delta\omega = \omega - E_{\rm exc}$, with ω the laser frequency, and $\rho(\epsilon)$ the quasiparticle DOS. The factor $\Big(1 - N_{\rm exc}(t)\Big)$, where $N_{\rm exc}(t) = N_{+1}(t) + N_0(t) + N_{-1}(t)$, stems from the fact that only one exciton per molecule can be created. The coupling constant γ depends on the strength of the absorption process as well as on the properties of the light beam, and can be parametrised as

$$\gamma = \alpha\, \mathcal{N}(\omega)\, \hbar\omega\,, \tag{S4.2}$$

where $\mathcal{N}(\omega)$ is the density of photons per molecule and α a parameter of dimension $\big[\text{time}^{-1}\big]$ that depends only on the system properties. Correspondingly, the equation of motion of the quasiparticle distribution is

$$\begin{aligned}
\dot{n}_{a\uparrow}(\epsilon, t) = \frac{\gamma}{2} \Big(1 - N_{\rm exc}(t)\Big) \Big[&- 2\, n_{a\uparrow}(\epsilon, t)\, \bar{n}_{a\downarrow}\big(\epsilon + \Delta\omega, t\big) - n_{a\uparrow}(\epsilon, t)\, \bar{n}_{a\uparrow}\big(\epsilon + \Delta\omega, t\big) \\
&+ 2\, \bar{n}_{a\uparrow}(\epsilon, t)\, n_{a\downarrow}\big(\epsilon - \Delta\omega, t\big) + \bar{n}_{a\uparrow}(\epsilon, t)\, n_{a\uparrow}\big(\epsilon - \Delta\omega, t\big)\Big] + I_{a\uparrow}(\epsilon, t)\,, \\
\dot{n}_{a\downarrow}(\epsilon, t) = \frac{\gamma}{2} \Big(1 - N_{\rm exc}(t)\Big) \Big[&- 2\, n_{a\downarrow}(\epsilon, t)\, \bar{n}_{a\uparrow}\big(\epsilon + \Delta\omega, t\big) - n_{a\downarrow}(\epsilon, t)\, \bar{n}_{a\downarrow}\big(\epsilon + \Delta\omega, t\big) \\
&+ 2\, \bar{n}_{a\downarrow}(\epsilon, t)\, n_{a\uparrow}\big(\epsilon - \Delta\omega, t\big) \;+ \bar{n}_{a\downarrow}(\epsilon, t)\, n_{a\downarrow}\big(\epsilon - \Delta\omega, t\big)\Big] + I_{a\downarrow}(\epsilon, t)\,,
\end{aligned} \tag{S4.3}$$

where $I_{a\sigma}(\epsilon, t)$ is the collision integral due to the residual interaction among quasiparticles. By writing Eq. (S4.1) and Eq. (S4.3) we have assumed that the spin-triplet quasiparticle-quasihole spectrum is that of weakly interacting quasiparticles. In other words, the paramagnon enhancement is taken into account only in the strength of the parameter α and not in the spectral redistribution of the joint quasiparticle-quasihole density of states.

Since the collision integrals conserve the quasiparticle energy per molecule, $\mathcal{E}(t)$, one can readily verify that the rate of its change is simply

$$\dot{\mathcal{E}}(t) = \sum_{a\sigma} \int d\epsilon\, \epsilon\, \rho(\epsilon)\, \dot{n}_{a\sigma}(\epsilon, t) = \Big(\omega - E_{\rm exc}\Big)\, \dot{N}(t)\,. \tag{S4.4}$$

On the contrary, the number of quasiparticles per molecule $\mathcal{N}(t)$ is assumed to be constant, even though, in reality, $\dot{\mathcal{N}}(t) = -\dot{N}_{\rm exc}(t)$. Eq. (S4.4) implies that below resonance, i.e. for $\omega < E_{\rm exc}$, the energy of quasiparticles diminishes, while above it increases. We emphasise that this result is due to our approximation $\mathcal{A}_{\rm exc}(\epsilon) = \delta\big(\epsilon - E_{\rm exc}\big)$ and to neglecting the reduction in quasiparticle number.

We solve the Boltzmann equations (S4.1) and (S4.3) assuming that the collision integral is so strong that local equilibrium is established at any instant of time during the pulse duration. We can therefore define an instantaneous value of the temperature $T(t)$. If we assume, besides the conservation of quasiparticle number, also particle-hole symmetry, then the chemical potential remains zero during the evolution. Under these assumptions it follows that

$$n_\sigma(\epsilon, t) = f\big(\epsilon, T(t)\big) \equiv \left(1 + \exp \frac{\epsilon}{T(t)}\right)^{-1} , \tag{S4.5}$$

namely the distribution at time t is the Fermi-Dirac one at temperature $T(t)$. Therefore, through equations (S4.1) and (S4.4), we have to solve

$$\begin{aligned} \dot{\mathcal{E}}(t) &= 6\, \frac{\dot{T}(t)}{T(t)^2} \int d\epsilon\, \epsilon^2\, \rho(\epsilon)\, f\Big(\epsilon, T(t)\Big) \Big[1 - f\Big(\epsilon, T(t)\Big)\Big] \\ &= 9\gamma\, \Delta\omega \int d\epsilon\, \rho(\epsilon)\, \rho(\epsilon + \Delta\omega)\, f\Big(\epsilon, T(t)\Big) \Big[1 - f\Big(\epsilon + \Delta\omega, T(t)\Big)\Big] , \end{aligned} \tag{S4.6}$$

which is a first order integro-differential equation for the instantaneous temperature $T(t)$ with initial condition $T(0) = T$, where T is the equilibrium value of the temperature before the pulse. This equation can be integrated numerically. In particular we used a Runge-Kutta based algorithm, and a semicircular $\rho(\epsilon)$ with half-bandwidth of 50 meV. The effective temperature at the end of the pulse with duration 300 fs is therefore $T_{\rm eff} = T\big(t = 300\ {\rm fs}\big)$.

In order to make contact with optical conductivity, we calculate in linear response the energy absorbed by the quasiparticle plus the exciton at frequency ω per unit time, in seconds, and per molecule, which, through (S4.1) and (S4.4) and relaxing the assumption $\mathcal{A}_{\rm exc}(\epsilon) = \delta\big(\epsilon - E_{\rm exc}\big)$, reads

$$\begin{aligned} \mathcal{W}(\omega) &= \hbar\omega\, \dot{N}(t) \simeq 9\, \gamma\, \hbar\omega \int d\epsilon_{\rm exc}\, \mathcal{A}_{\rm exc}\big(\epsilon_{\rm exc}\big) \int d\epsilon\, \rho(\epsilon)\, \rho(\epsilon + \omega - \epsilon_{\rm exc})\, f(\epsilon, T)\, \bar{f}\big(\epsilon + \omega - \epsilon_{\rm exc}, T\big) \\ &\equiv 9\, \alpha\, \hbar^2\, \omega^2\, \mathcal{N}(\omega)\, J(\omega, T) , \end{aligned} \tag{S4.7}$$

where $\bar{f}(\epsilon, T) = 1 - f(\epsilon, T)$. The density of the electromagnetic field at frequency ω and per molecule is

$$E_{\rm EMF}(\omega) = \hbar\omega\, \mathcal{N}(\omega) ,$$

so that, since in the units of Ref. [19]

$$1\,\Omega\,\mathrm{cm} = 0.423\,\mathrm{ps} \;\rightarrow\; \frac{\hbar}{\Omega\,\mathrm{cm}} = 1.56\ \mathrm{meV}\,,$$

the absorption rate in unit energy is

$$\frac{\hbar}{\tau(\omega)} \simeq 1.56\ \mathrm{meV}\,\sigma_1(\omega)\left[\Omega^{-1}\,\mathrm{cm}^{-1}\right] = \frac{\hbar\mathcal{W}(\omega)}{E_{\mathrm{EMF}}(\omega)} = 9\,\hbar\alpha\,\hbar\omega\,J(\omega,T)\,. \tag{S4.8}$$

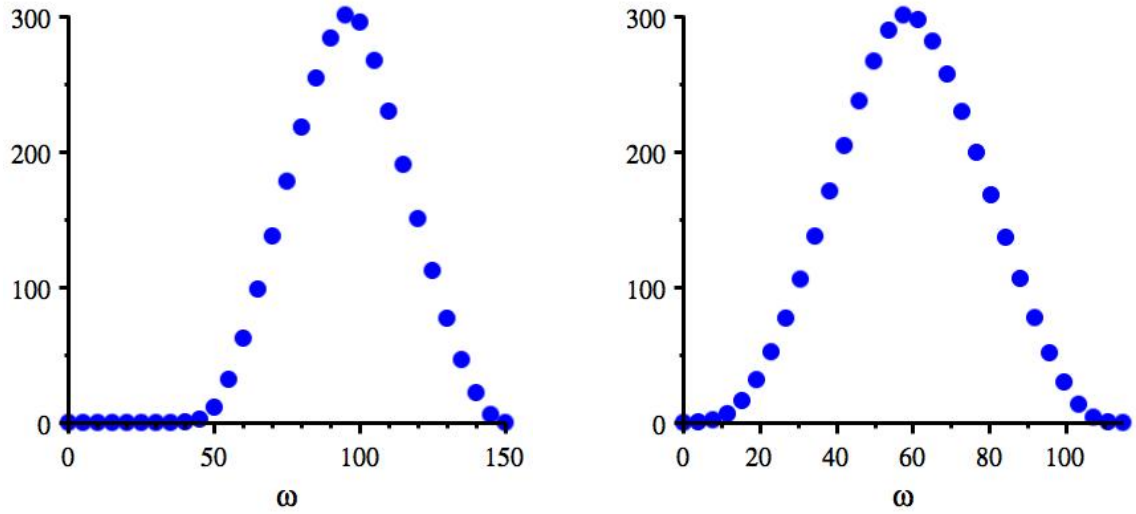

Figure S4.1: Calculated contribution of the excitonic absorption to optical conductivity at $T =$ 25 K assuming semicircular $\rho(\epsilon)$ and $\mathcal{A}_{\mathrm{exc}}(\epsilon)$, the former with half-bandwidth 50 meV, left panel, and 40 meV, right panel, and the latter with a tenth of it. The exciton is centred at 50 meV, left panel, and 20 meV, right panel.

In the left panel of Fig. S4.1 we plot the excitonic contribution to optical conductivity calculated at $T = 25$ K assuming semicircular $\rho(\epsilon)$ and $\mathcal{A}_{\mathrm{exc}}(\epsilon)$, the former with half-bandwidth $D = 50$ meV and the latter with a tenth of it and centred at $E_{\mathrm{exc}} = 50$ meV. The fitting parameter is such as to give a peak of $300\left[\Omega^{-1}\,\mathrm{cm}^{-1}\right]$, which we find corresponds to $\hbar\alpha = 2.2\,D$. In comparison with the experimental data, the curve is shifted to higher frequency. A better fit could be obtained with smaller values of $E_{\mathrm{exc}} = 20$ meV and $D = 40$ meV, right panel of the figure. We repute those values a bit unphysical and believe that the higher peak frequency as compared with experiment is rather due to our approximation of the dynamical spin susceptibility with that of weakly interacting quasiparticles.
The experiment of Ref. [19] is performed at fixed fluence, which implies at fixed value of

$E_{\mathrm{EMF}}(\omega) = \hbar\omega\,\mathcal{N}(\omega)$. A fluence of 1 mJ cm^{-2} with a penetration depth of 220 nm [19] would correspond to an energy of the electromagnetic field per molecule of around $E_{\mathrm{EMF}}(\omega) = 207$ meV. Given the crudeness of our modelling and the neglect of other absorption processes, in the calculation we took a smaller $E_{\mathrm{EMF}}(\omega) = 100$ meV, which provides results closer to the experiment.

References

[1] N. Troullier and José Luís Martins. Structural and electronic properties of C_{60}. *Phys. Rev. B*, 46:1754–1765, Jul 1992.

[2] A. V. Nikolaev and K. H. Michel. Molecular terms, magnetic moments, and optical transitions of molecular ions $C_{60}^{m\pm}$. *The Journal of Chemical Physics*, 117(10):4761–4776, 2002.

[3] Nicola Manini and Erio Tosatti. Exact zero-point energy shift in the $e\bigotimes$(nE), $t\bigotimes$(nH) many-modes dynamic Jahn-Teller systems at strong coupling. *Phys. Rev. B*, 58:782–790, Jul 1998.

[4] Naoya Iwahara, Tohru Sato, Kazuyoshi Tanaka, and Liviu F. Chibotaru. Vibronic coupling in C_{60}^{-} anion revisited: Derivations from photoelectron spectra and dft calculations. *Phys. Rev. B*, 82:245409, Dec 2010.

[5] Massimo Capone, Michele Fabrizio, Claudio Castellani, and Erio Tosatti. *Colloquium* : Modeling the unconventional superconducting properties of expanded A_3C_{60} fullerides. *Rev. Mod. Phys.*, 81:943–958, Jun 2009.

[6] P. Bhyrappa, Parimal Paul, John Stinchcombe, Peter D. W. Boyd, and Christopher A. Reed. Synthesis and electronic characterization of discrete buckminsterfulleride salts: C602- and c603-. *Journal of the American Chemical Society*, 115(23):11004–11005, 1993.

[7] Christopher A. Reed and Robert D. Bolskar. Discrete fulleride anions and fullerenium cations. *Chemical Reviews*, 100(3):1075–1120, 2000. PMID: 11749258.

[8] Peter D. W. Boyd, P. Bhyrappa, Parimal Paul, John Stinchcombe, Robert Bolskar, Yongping Sun, and Christopher A. Reed. The c602- fulleride ion. *Journal of the American Chemical Society*, 117(10):2907–2914, 1995.

[9] William H. Green, Sergiu M. Gorun, George Fitzgerald, Patrick W. Fowler, Arnout Ceulemans, and Bruno C. Titeca. Electronic structures and geometries of c60 anions via density functional calculations. *The Journal of Physical Chemistry*, 100(36):14892–14898, 1996.

[10] V. Brouet, H. Alloul, S. Garaj, and L. Forró. Persistence of molecular excitations in metallic fullerides and their role in a possible metal to insulator transition at high temperatures. *Phys. Rev. B*, 66:155124, Oct 2002.

[11] V. Brouet, H. Alloul, S. Garaj, and L. Forró. Gaps and excitations in fullerides with partially filled bands: Nmr study of na_2c_{60} and k_4c_{60}. *Phys. Rev. B*, 66:155122, Oct 2002.

[12] Y. Maniwa, N. Muroga, N. Sato, H. Tou, H. Shimoda, Y. Iwasa, H. Mitani, K. Kikuchi, S. Suzuki, Y. Achiba, M. Kosaka, K. Tanigaki, X. Chen, and M. M. Labes. ^{13}C. *Phys. Rev. B*, 58:11603–11606, Nov 1998.

[13] S. S. Naghavi, M. Fabrizio, T. Qin, and E. Tosatti. Nanoscale orbital excitations and the infrared spectrum of a molecular mott insulator: A15-cs3c60. *Nanoscale*, 8:17483–17488, 2016.

[14] Robert D. Bolskar, Sean H. Gallagher, Robert S. Armstrong, Peter A. Lay, and Christopher A. Reed. Analysis of the near-infrared spectra of c60. *Chemical Physics Letters*, 247(1):57 – 62, 1995.

[15] S. Tomita, J. U. Andersen, E. Bonderup, P. Hvelplund, B. Liu, S. Brøndsted Nielsen, U. V. Pedersen, J. Rangama, K. Hansen, and O. Echt. Dynamic jahn-teller effects in isolated c_{60}^- studied by near-infrared spectroscopy in a storage ring. *Phys. Rev. Lett.*, 94:053002, Feb 2005.

[16] S. Wehrli and M. Sigrist. Jahn-teller effect versus hund's rule coupling in c_{60}^{N-}. *Phys. Rev. B*, 76:125419, Sep 2007.

[17] Ian D. Hands, Janette L. Dunn, Colin A. Bates, Michael J. Hope, Steve R. Meech, and David L. Andrews. Vibronic interactions in the visible and near-infrared spectra of c_{60}^- anions. *Phys. Rev. B*, 77:115445, Mar 2008.

[18] Haifa S. Alqannas, Andrew J. Lakin, Joseph A. Farrow, and Janette L. Dunn. Interplay between coulomb and jahn-teller effects in icosahedral systems with triplet electronic states coupled to h-type vibrations. *Phys. Rev. B*, 88:165430, Oct 2013.

[19] M. Mitrano, A. Cantaluppi, D. Nicoletti, S. Kaiser, A. Perucchi, S. Lupi, P. Di Pietro, D. Pontiroli, M. Riccò, S. R. Clark, D. Jaksch, and A. Cavalleri. Possible light-induced superconductivity in k3c60 at high temperature. *Nature*, 530(7591):461–464, 02 2016.